Workshop on Unbound Nuclei, Pisa, Italy, November 3-5, 2008

Resonances and how they decay into three fragments

A.S. Jensen [1], R. Álvarez-Rodríguez [1], E. Garrido [2],
D.V. Fedorov [1], H.O.U. Fynbo [1], O.S. Kirsebom [1]

[1]IFA, University of Aarhus, DK-8000 Aarhus C
[2]Instituto de Estructura de la Materia, CSIC, E-28006 Madrid

CONTENT:

1. The problem of three-body decay of a resonance
2. Three-body model for many particles
3. Illustration by the ^{9}Be$(5/2^{-})$-resonance
4. R-matrix analysis: When is it meaningful, ^{12}C$(1^{+}, 2^{-}, 4^{-})$
5. Requirements for accuracy, ^{12}C(0^{+}) and ^{17}Ne$(3/2^{-})$
6. Efimov effect: ^{11}Li(1^{-})
7. Further illustrations, ^{6}Be$(0^{+}, 2^{+})$
8. Summary and conclusions

Which problem do we want to solve?

Initial state is prepared in an experiment

The oberservables are three particles emerging in a final state
measured accurately and kinematically complete

What can we say about the initial state and/or the process?

For two particles in the final state (like α-emission),
energy and momentum conservation determine the final state energy

For three particles in the final state, the energy and momentum
distributions are continuous, similar to beta-decay

What are the difficulties?

The many-body problem at small distances
contracts to a three-body problem at large distance

Both small and large distances are crucial

Decay process and hence a continuum problem

Both Coulomb + short-range interactions are important

The asymptotic large-distance behavior can vary as:
individual two-body, coherent two-body,
three-body structures, mixing of these

Comparison to measurements is difficult since
R-matrix analysis derives "observed" values, not observables
ex. sequential decay branching ratios and "simulated"
momentum distributions filtered through experimental parameters

Formulation and Method

Set up a model to compute momentum distributions of decay fragments

Assume population of resonance state, in reaction or beta decay, independent of previous history (not necessary but simplification)

Compute three-body resonance wavefunction in coordinate space, Fourier transform to get observable momentum distributions

Accurate large-distance coordinate space properties are crucial

Three-body method of adiabatic hyperspherical expansion is used

Complex scaling facilitates the large-distance boundary condition and provides distinction between sequential and direct decay

Hamiltonian

$(\Sigma_i T_i - T_{cm} + \Sigma_{i<k} V_{ik} + V_{3b})\,\Psi = E\Psi \quad$ where $\{i,k\} \in \{1,2,3\}$

Coordinates:
$\boldsymbol{r_{ik}} = \boldsymbol{r_k} - \boldsymbol{r_i}$ is the vector connecting particle i and k

$(\boldsymbol{x}, \boldsymbol{y})$ are mass scaled Jacobi coordinates

$x^2 = r_{ik}^2 \;\; \frac{m_i m_k}{m(m_i+m_k)}$, $\qquad y^2 = r_{j,ik}^2 \;\; \frac{m_j(m_i+m_k)}{m(m_i+m_k+m_j)}$

$\rho^2 = x^2 + y^2 = \frac{1}{m(m_i+m_k+m_j)} \;\; \sum_{i<j} m_i m_j r_{ij}^2$

$\Omega = \{\Omega_x, \Omega_y, \alpha\}$ are directions of $(\boldsymbol{x}, \boldsymbol{y})$ and $\tan\alpha = \frac{x}{y}$

Complex scaling: $\rho \to \rho\exp(i\theta)$

Procedure

Choose interactions, solve Faddeev equations for each ρ

Obtain angular eigenvalues λ_n and eigenfunctions $\{\Phi_n(\rho,\Omega)\}$

Three-body resonance state Ψ is given by the Faddeev decomposition

$$\Psi(\boldsymbol{x},\boldsymbol{y}) = \Psi(\rho,\Omega) = \sum_n f_n(\rho)\Phi_n(\rho,\Omega) =$$
$$\sum_n f_n(\rho)\left(\phi_{12}^{(n)}(\rho,\Omega) + \phi_{13}^{(n)}(\rho,\Omega) + \phi_{23}^{(n)}(\rho,\Omega)\right)$$

The Fourier transform $\tilde{\Psi}$ of the coordinate space resonance wavefunction Ψ has the same angular dependence as Ψ

The ρ-dependence is exchanged with a Breit-Wigner shape:

$\frac{\Psi(\rho_{max},\Omega_k)}{\kappa^2-\kappa_0^2}$, κ_0 is related to the resonance energy, $\Omega_k = \{\Omega_{kx},\Omega_{ky},\alpha_k\}$

Observables are found by absolute square and integration

Crucial Ingredients

Faddeev decomposition

Large hyperharmonic basis for each Faddeev component $\phi_{ik}^{(n)}(\rho, \Omega)$

Accurate large-distances:
outgoing waves of radial wavefunctions f_n

Three-body resonance tuned by use of the three-body potential V_{3b}

The small-distance boundary condition defined in three-body space

Many-body degrees of freedom contract to three particles at the surface

For α-emission two fragments appear outside the core

Here three-body structure outside the core nucleus

Sequential and/or Direct Decay

Two different decay mechanisms connecting initial and final states

This "decay path" is not a quantum mechanical observable

Distinction is only possible in special limits

Basis for Sequential Decay:
Two-body basis $\otimes$ third particle in the continuum

Basis for Direct Decay: Three-body continuum wavefunctions

Observables can be described in any complete basis set

One may be better suited

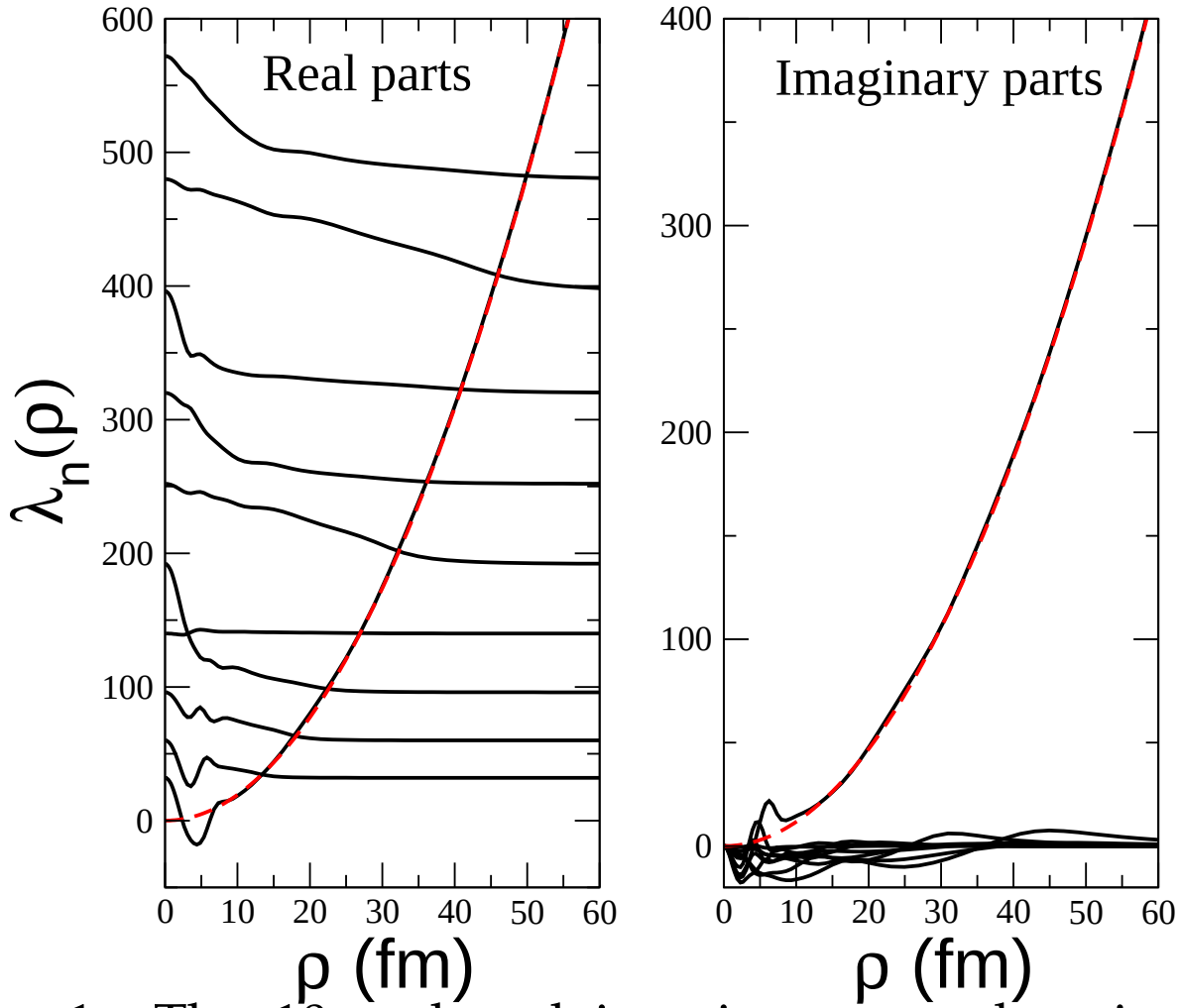

Figure 1: The 10 real and imaginary angular eigenvalues as function of ρ for 0^+ for three bosons interacting by d-waves. The two-body systems have a d-resonance at 4.53 MeV with a width of 2.36 MeV ($\theta_R = 0.127$). The red curves are the real and imaginary parts of the parabola $2m|E|\rho^2 \exp(2i(\theta - \theta_R))/\hbar^2$. The complex scaling angle $\theta = 0.4$.

"Red" resonance population decreases at crossings vanishing for large ρ
Direct and sequential means: nothing or everything is on this potential
Gradual change, artificial, basis choice

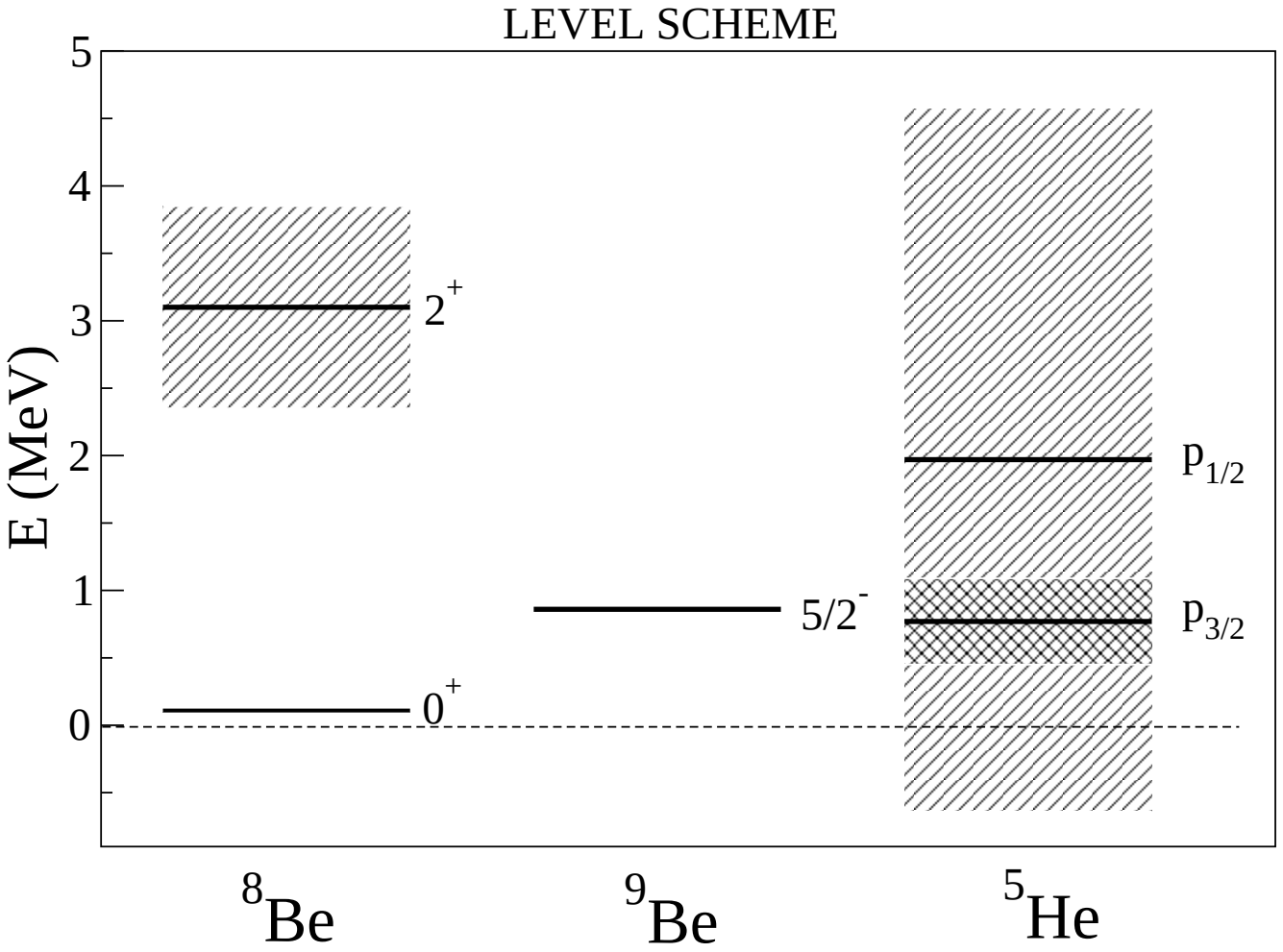

Figure 2: The lowest levels of ^{8}Be and ^{5}He through which the sequential decay of the ^{9}Be$(5/2^{-})$-resonance should proceed.

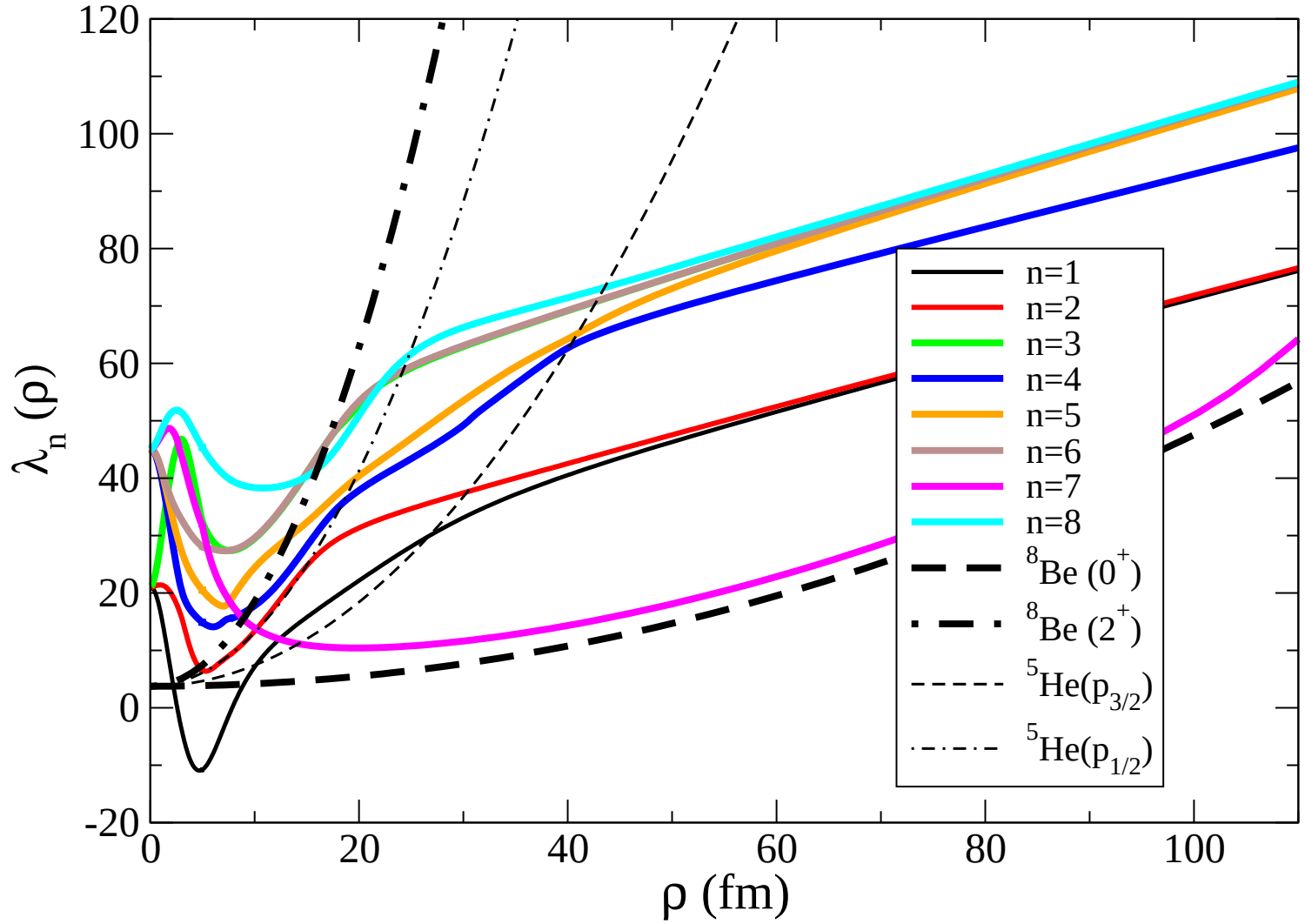

Figure 3: The real part of the lowest angular eigenvalues for the ^{9}Be$(5/2^-)$-resonance. The thick and thin dashed parabolic curves are the asymptotics corresponding to the lowest $(0^+,2^+)$ and $(p_{3/2},p_{1/2})$ resonances for ^{8}Be and ^{5}He, respectively.

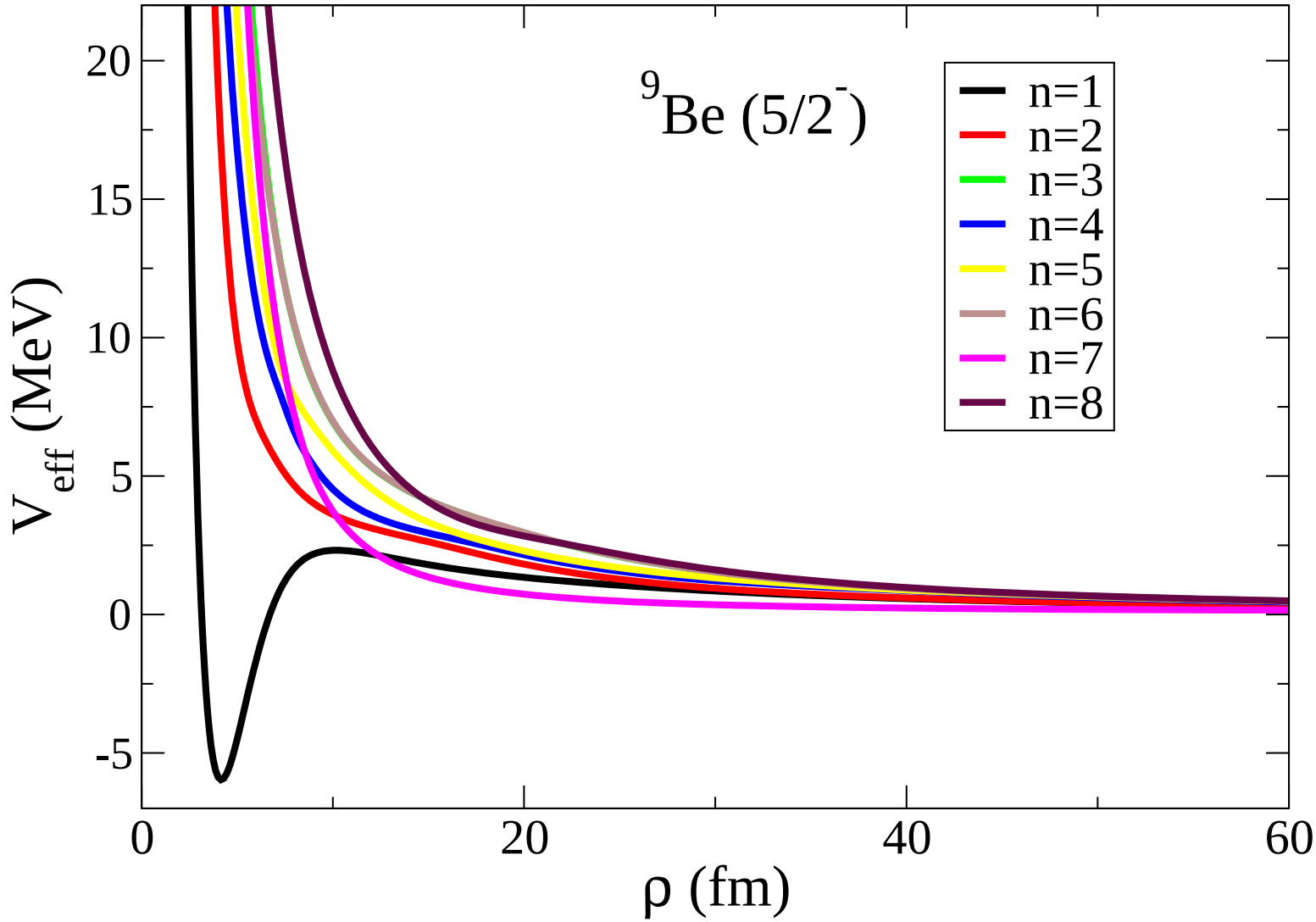

Figure 4: The lowest real potentials, including the three-body potential, for the ^{9}Be$(5/2^-)$-resonance as function of hyperradius.

The lowest has a pocket holding the resonance at the measured excitation energy of 2.429 MeV or 0.856 MeV above the three-particle breakup threshold.

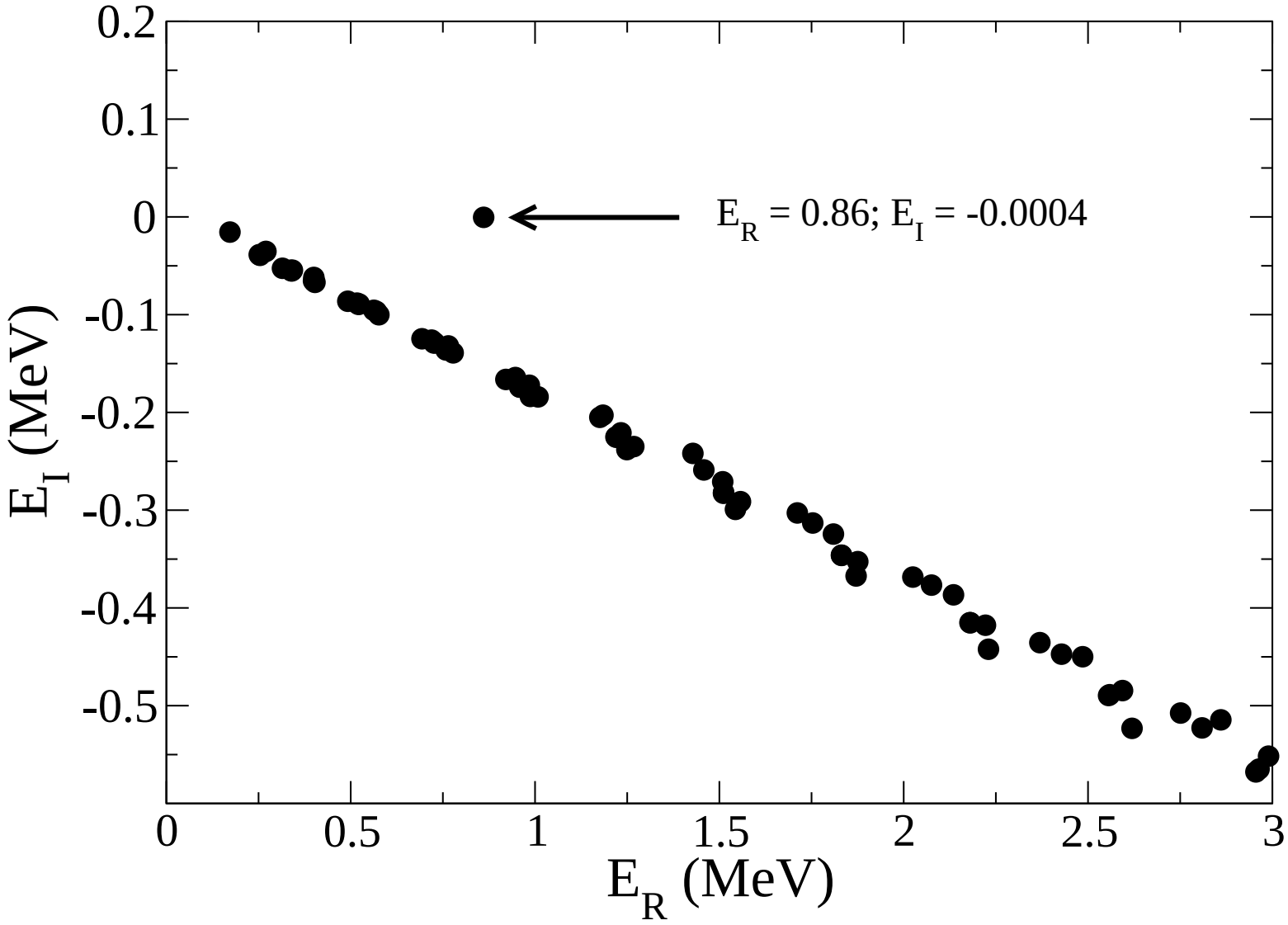

Figure 5: The energy spectrum with real and imaginary values for the discretized rotated continuum, and the resonance at the correct point.

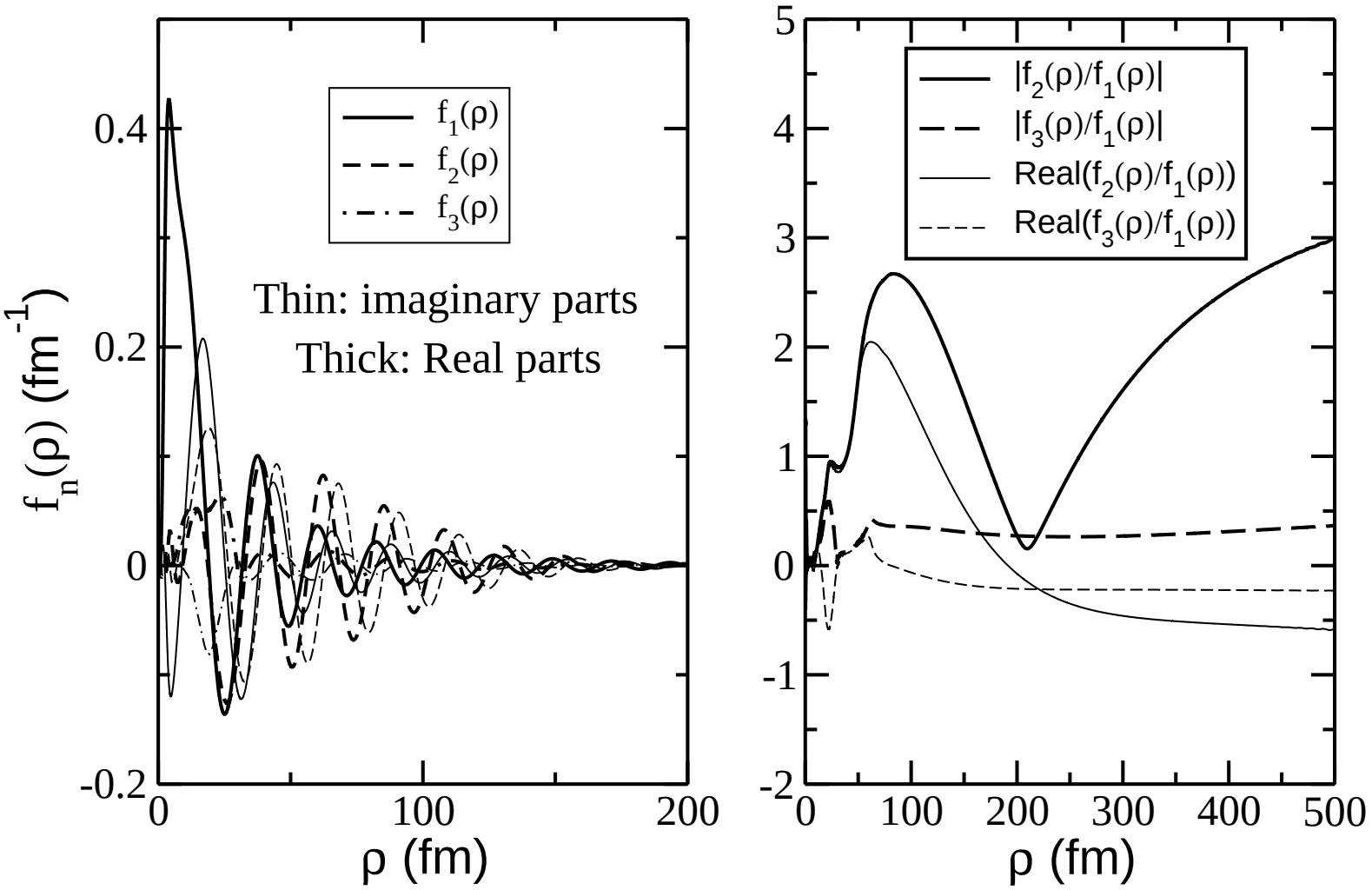

Figure 6: The radial wavefunctions for the second 2^+-resonance in ^{6}Li. The scaling angle is $\theta = 0.10$.

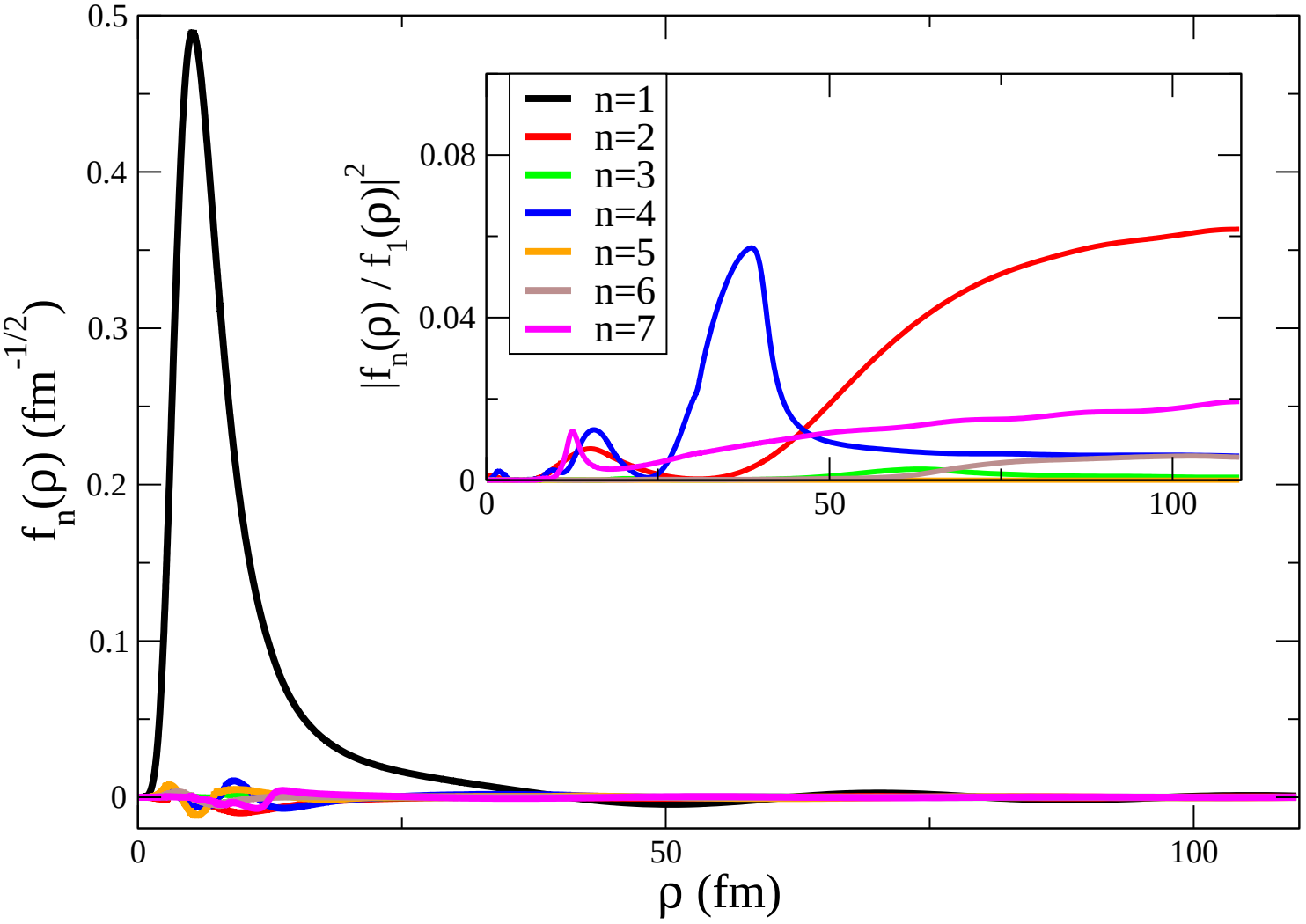

Figure 7: The dominating (first) radial wavefunction f_1 as function of ρ for the ^{9}Be$(5/2^-)$-resonance, and in the insert the ratios $|f_n/f_1|^2$.

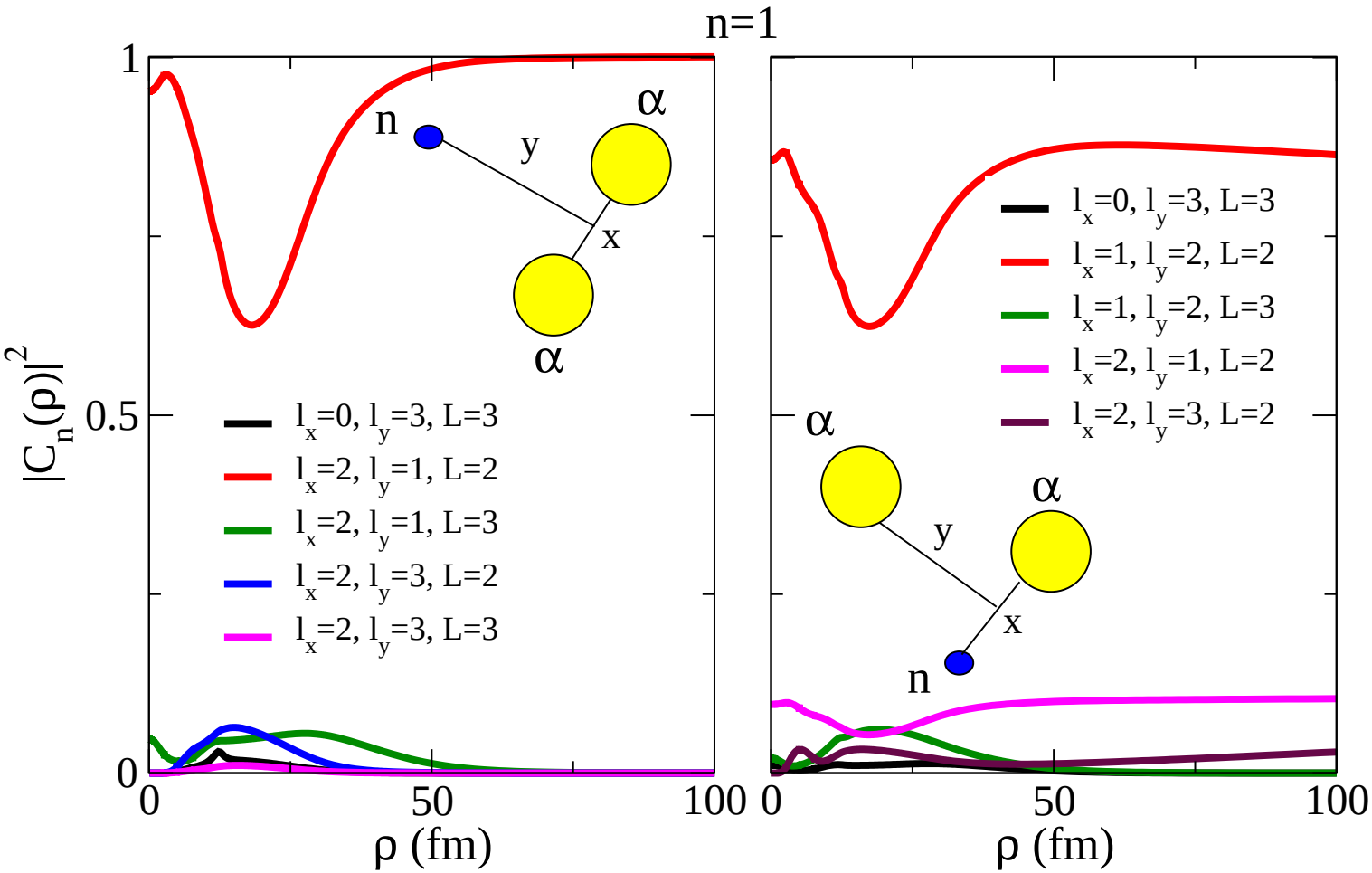

Figure 8: The partial wave decomposition in the two Jacobi coordinates of the first adiabatic potential for the ^{9}Be$(5/2^-)$-resonance.

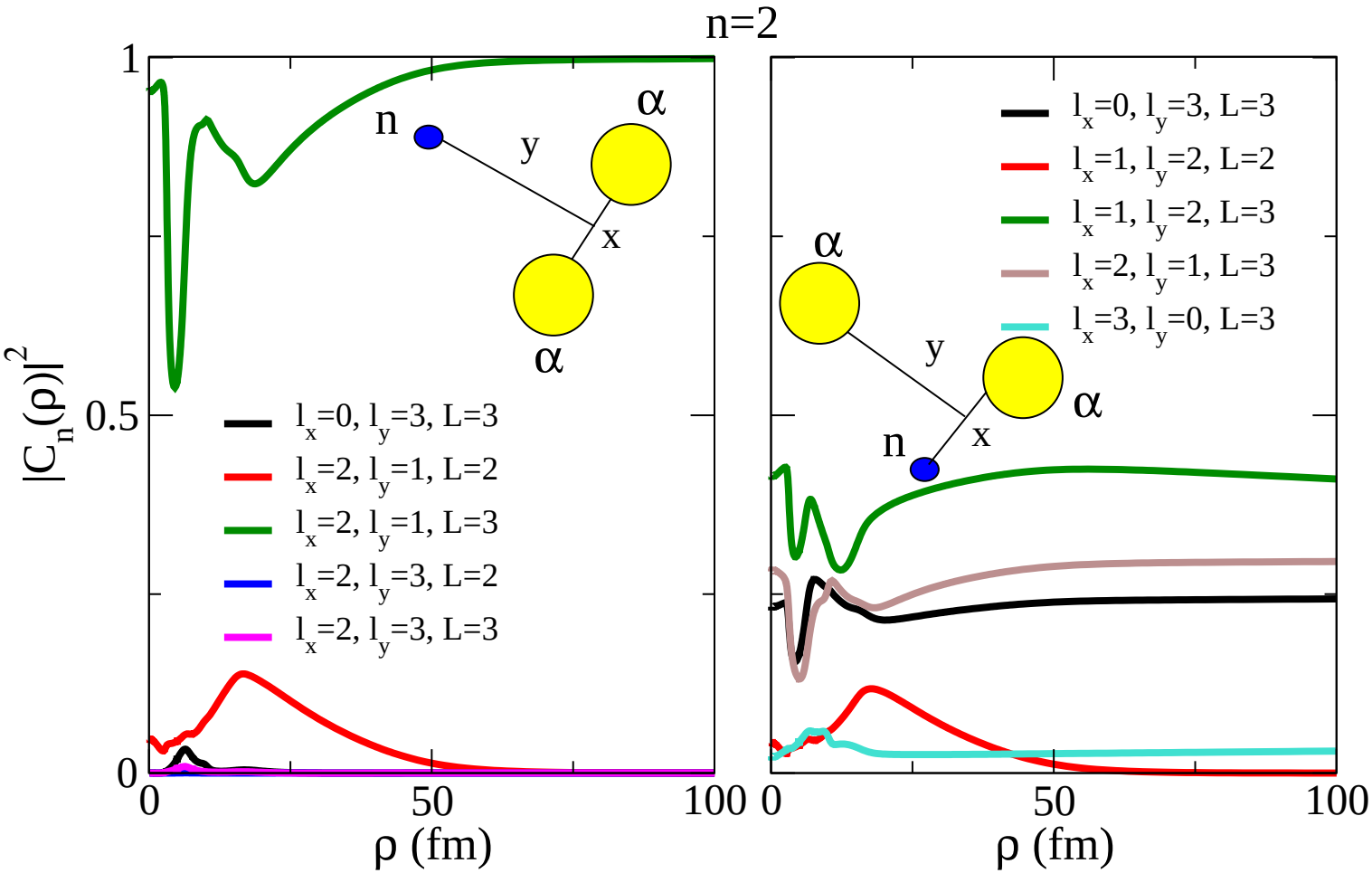

Figure 9: The partial wave decomposition in the two Jacobi coordinates of the second adiabatic potential for the ^{9}Be$(5/2^-)$-resonance.

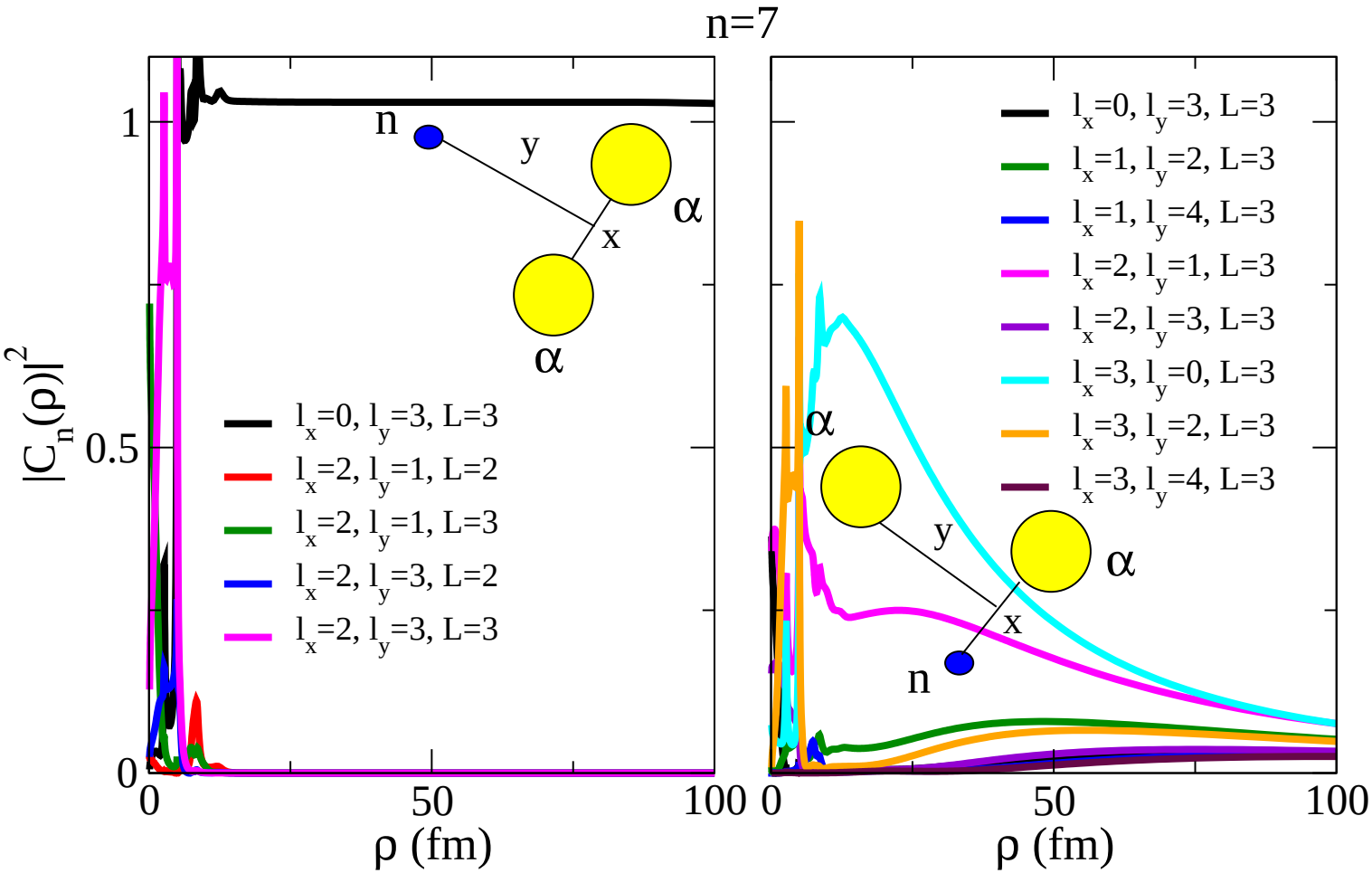

Figure 10: The partial wave decomposition in the two Jacobi coordinates of the seventh adiabatic potential for the ^{9}Be$(5/2^-)$-resonance.

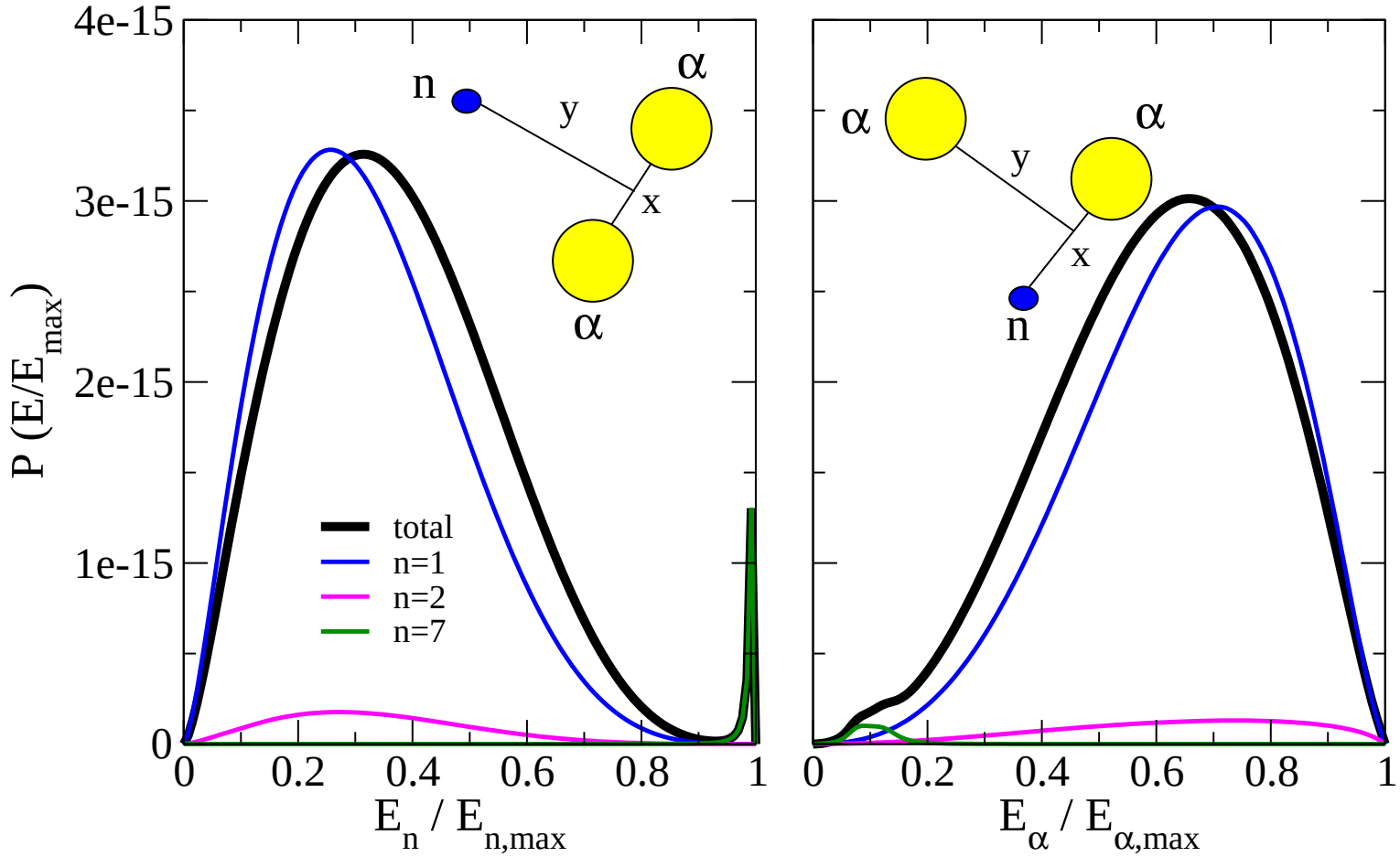

Figure 11: The energy spectra of the emitted neutron and α-particles. The individual contributions from the first, second and seventh adiabatic components are shown.

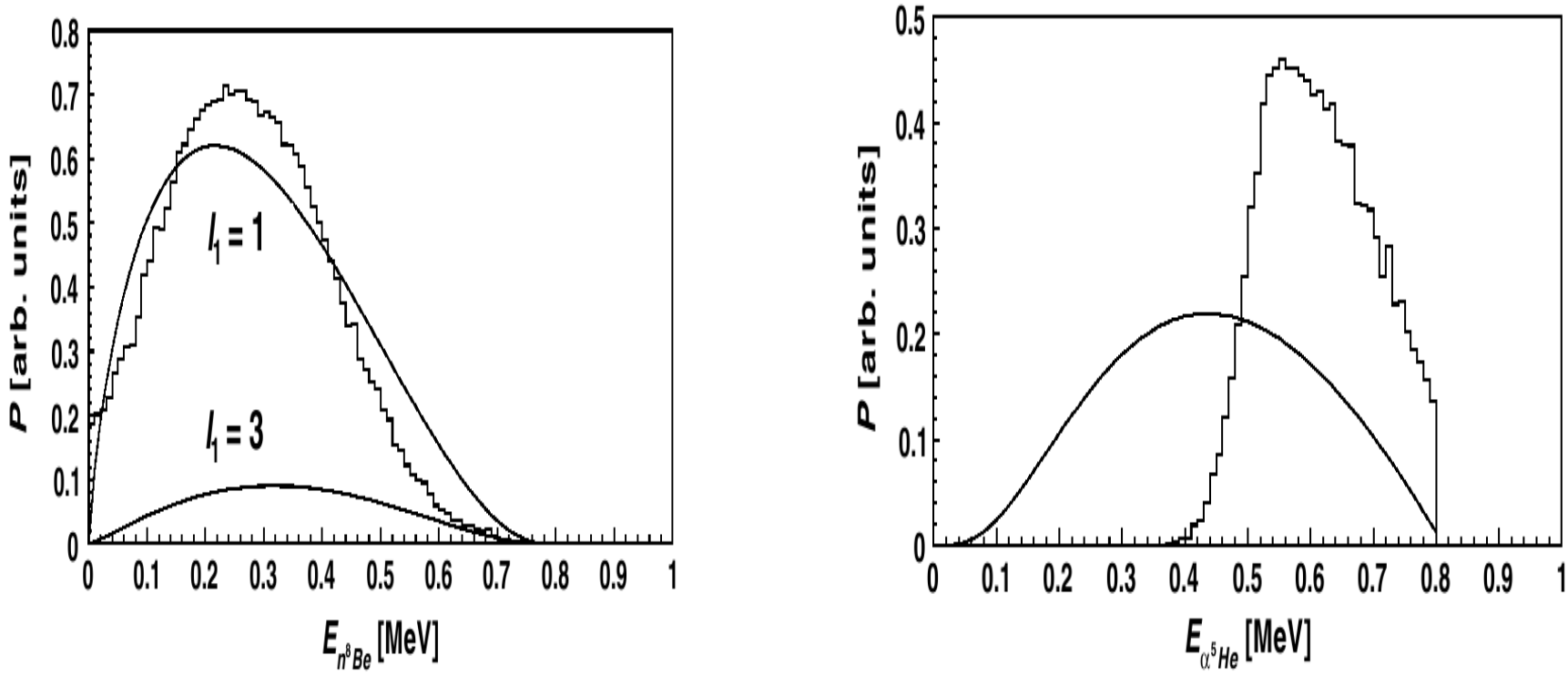

Figure 12: The measured [20] (P. Papka et al.) energy spectra of the emitted neutron and α-particles.

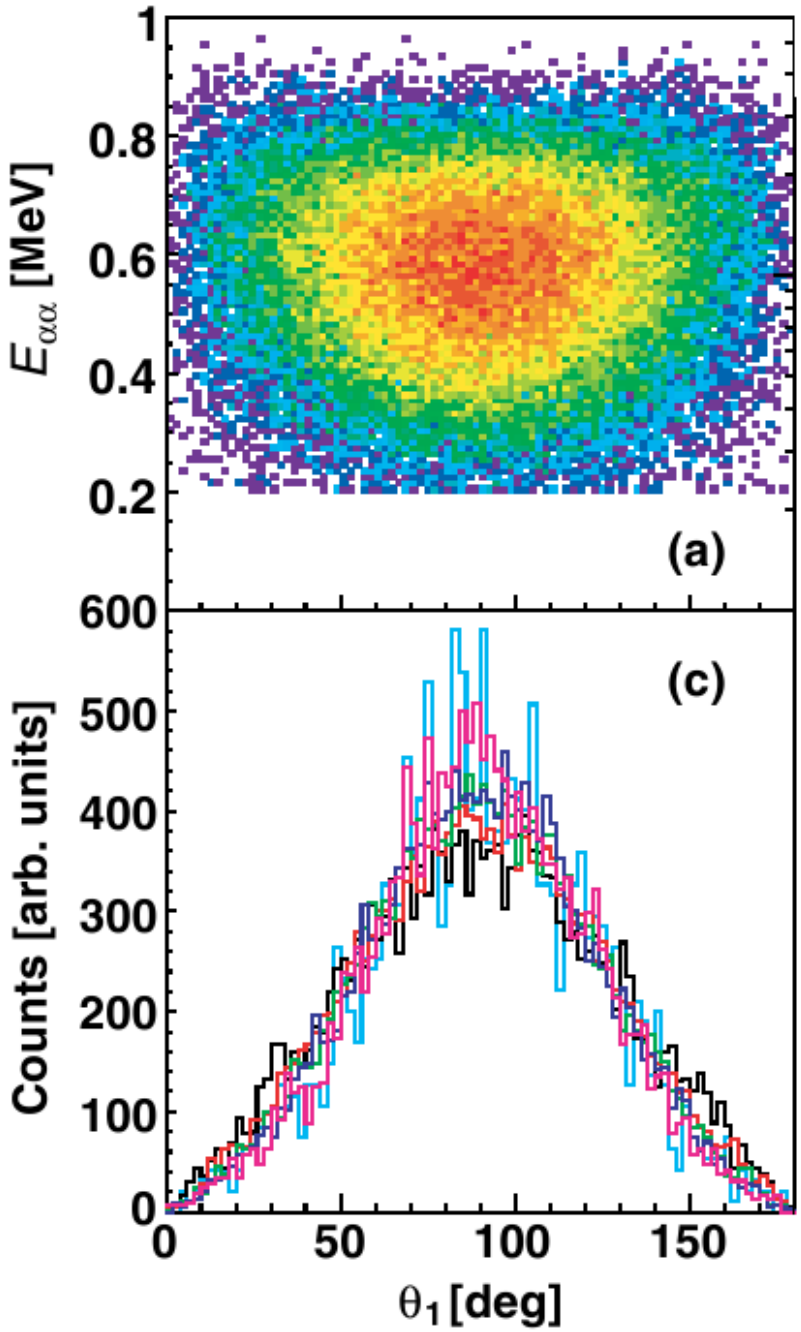

Figure 13: The measured [20] (P. Papka et al.) relative energy distributions of the two α-particles as function of the angle θ_1 between the $\alpha - \alpha$ momentum and the momentum of the emitted neutron.

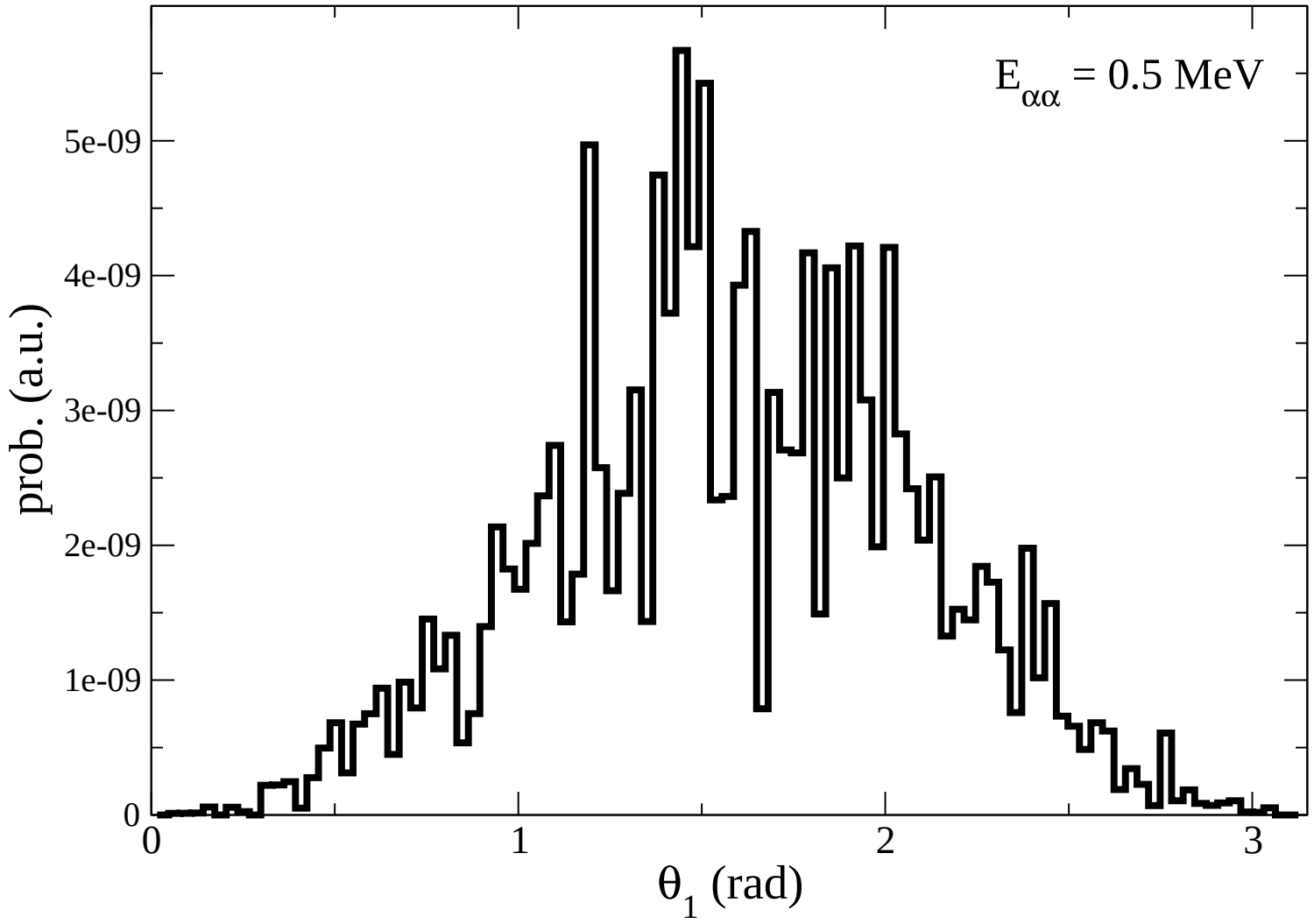

Figure 14: The computed probability for two α-particles with a relative energy of 0.5 MeV emerging in the direction defined by the angle θ_1 between the $\alpha - \alpha$ momentum and the direction of the emitted neutron.

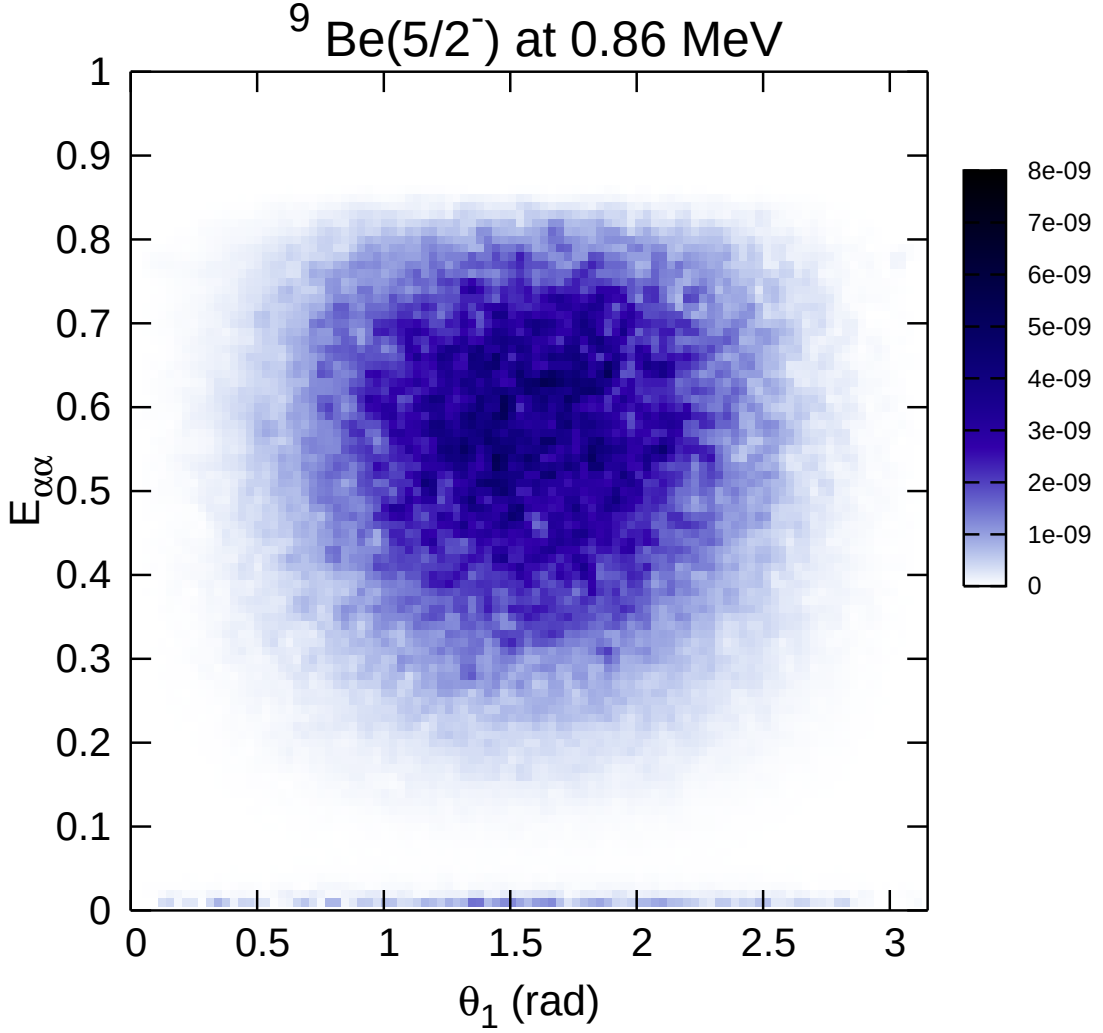

Figure 15: The computed relative energy distributions of the two α-particles as function of the angle θ_1 between the $\alpha - \alpha$ momentum and direction of the emitted neutron.

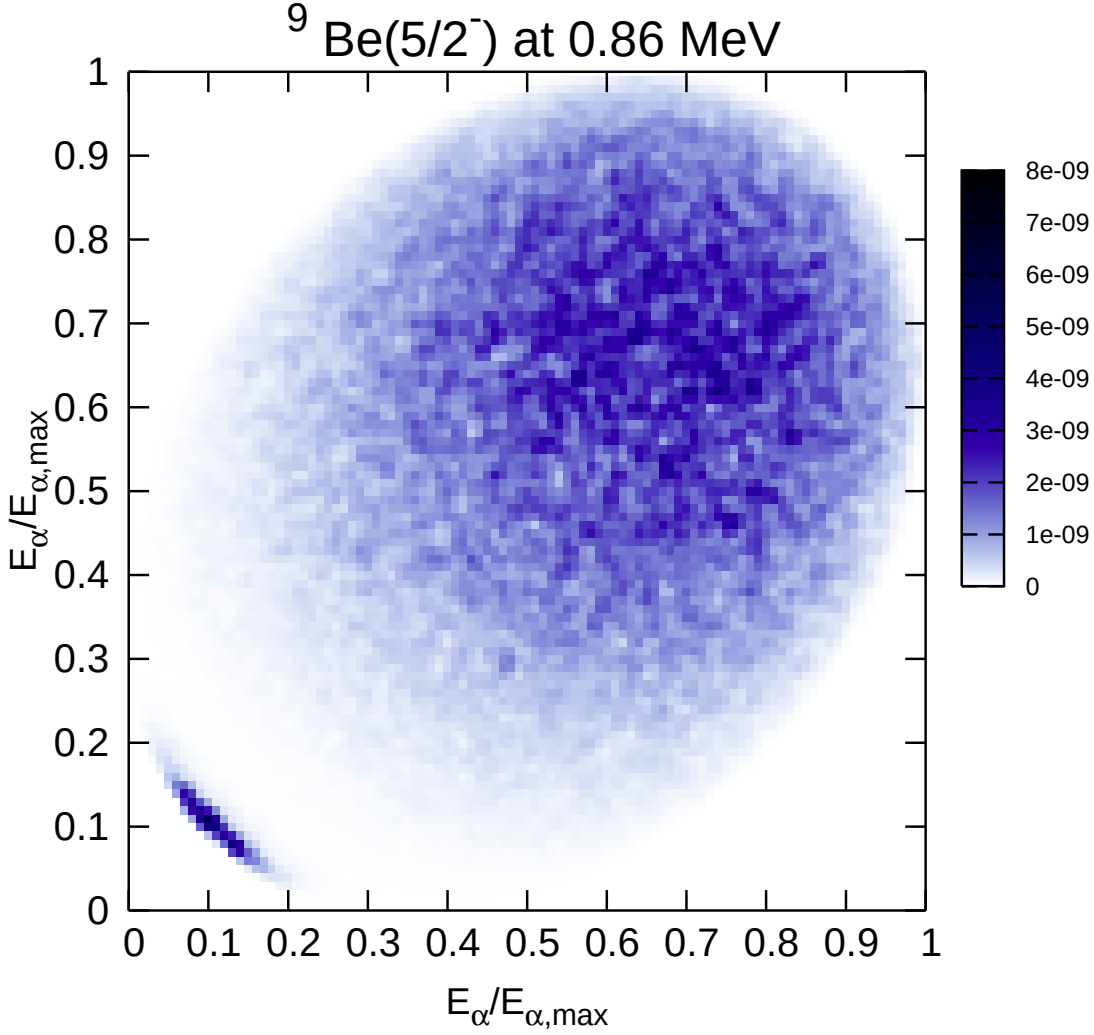

Figure 16: The $\alpha - \alpha$ energy distribution.

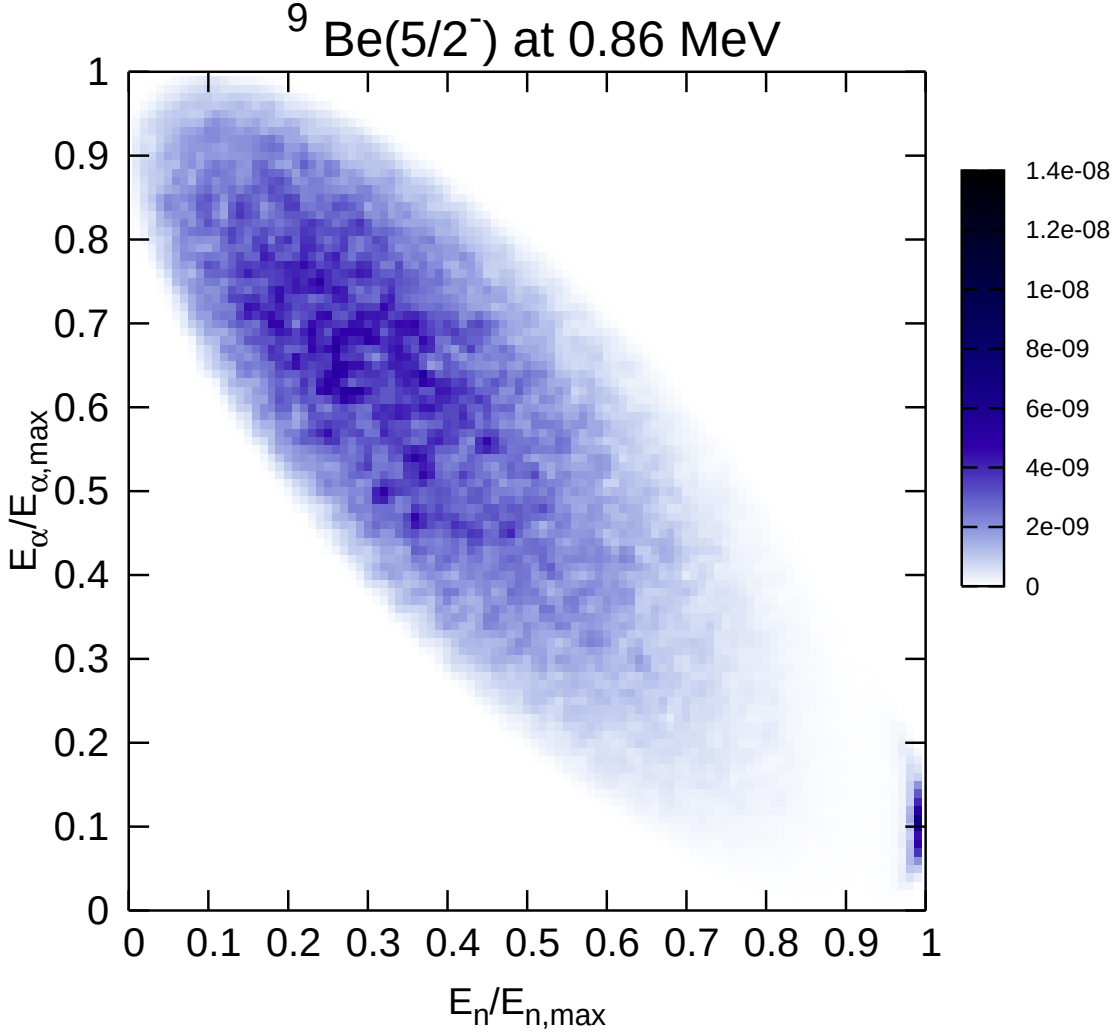

Figure 17: The neutron-α energy distribution.

R-matrix analysis

$$f_{x,y} \propto \frac{\sqrt{\Gamma_y \Gamma_{2r} / \sqrt{E_y E_x}}}{E_{2r} - i\frac{1}{2}\Gamma_{2r} - E_x - \gamma_2^2[S_{\ell_x}(E_x) - S_{\ell_x}(E_{2r})]}$$

Three-body resonance energy: $E_{3r} - i\Gamma_{3r}/2$
Two-body resonance energy: $E_{2r} - i\Gamma_{2r}/2$
Two-body orbital angular momentum: ℓ_x
First emitted particle energy: $E_y = E_{3r} - E_x$
Barrier penetrability: $P_{\ell_y}(E)$ where $\Gamma_y = 2P_{\ell_y}(E)\gamma^2$
Reduced width: γ^2, and Shift function: S_ℓ

With Bose symmetry:

$$\begin{aligned} f &= \sum_{x,y} \sum_{m_x \ell_y} (\ell_y M - m_b j_x m_x | JM) Y_{\ell_y}^{M-m_b}(\Theta_y, \Phi_y) \\ &\times Y_{\ell_x}^{m_x}(\theta_x, \phi_x) f_{x,y}\, e^{i(\omega_{\ell_y} - \phi_{\ell_y})} e^{i(\omega_{\ell_x} - \phi_{\ell_x})} \end{aligned}$$

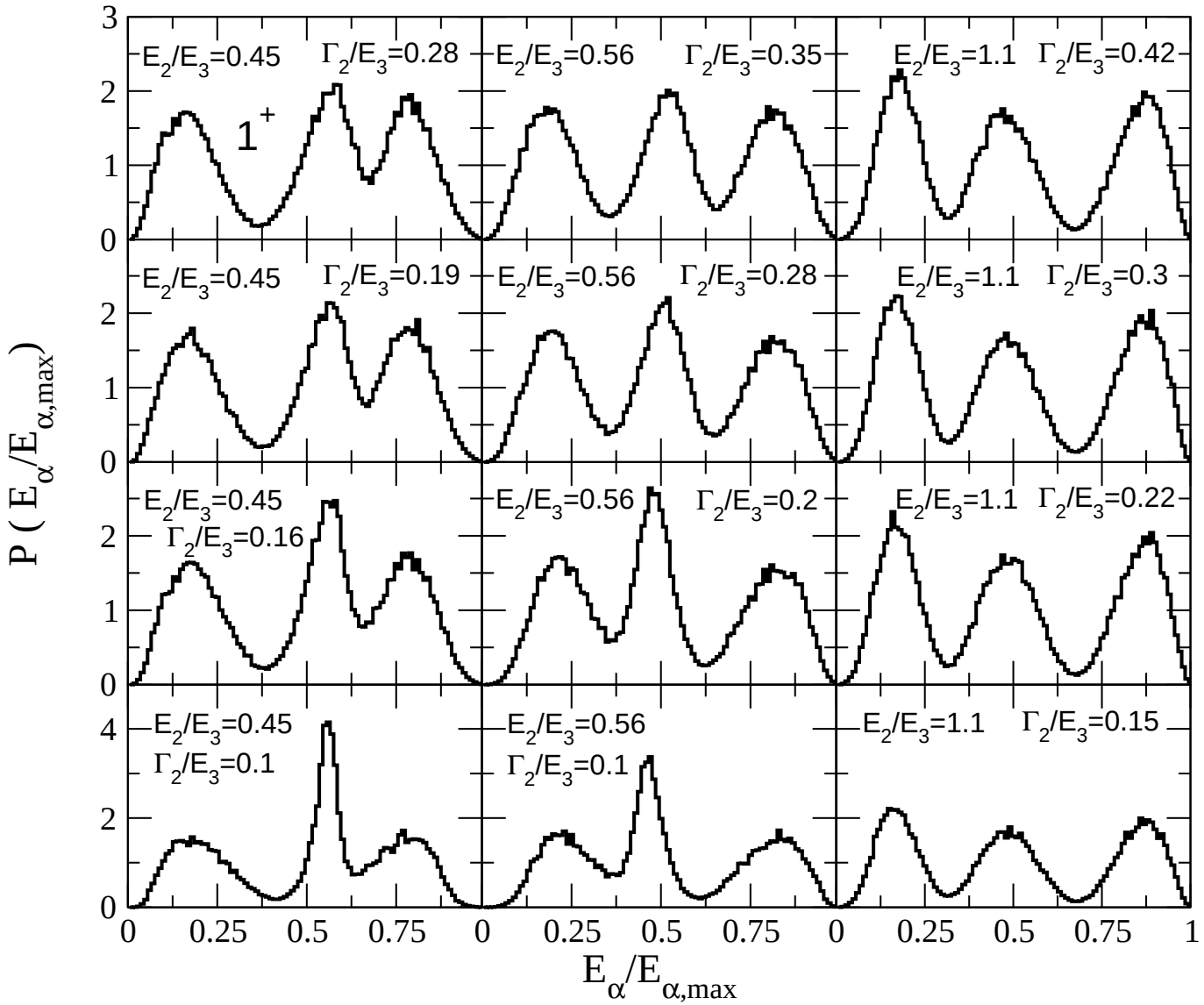

Figure 18: Single-alpha energy distributions from R-matrix analysis for decay into three α-particles of the 1^+ resonance in ^{12}C at an energy of $E_3 = 5.43$ MeV and a partial width of about 18 keV. The energies and widths of the intermediate 2^+ resonance in ^{8}Be are varied in the simulations as specified in the panels. The maximum energy $E_{\alpha,max} = 2E_3/3$.

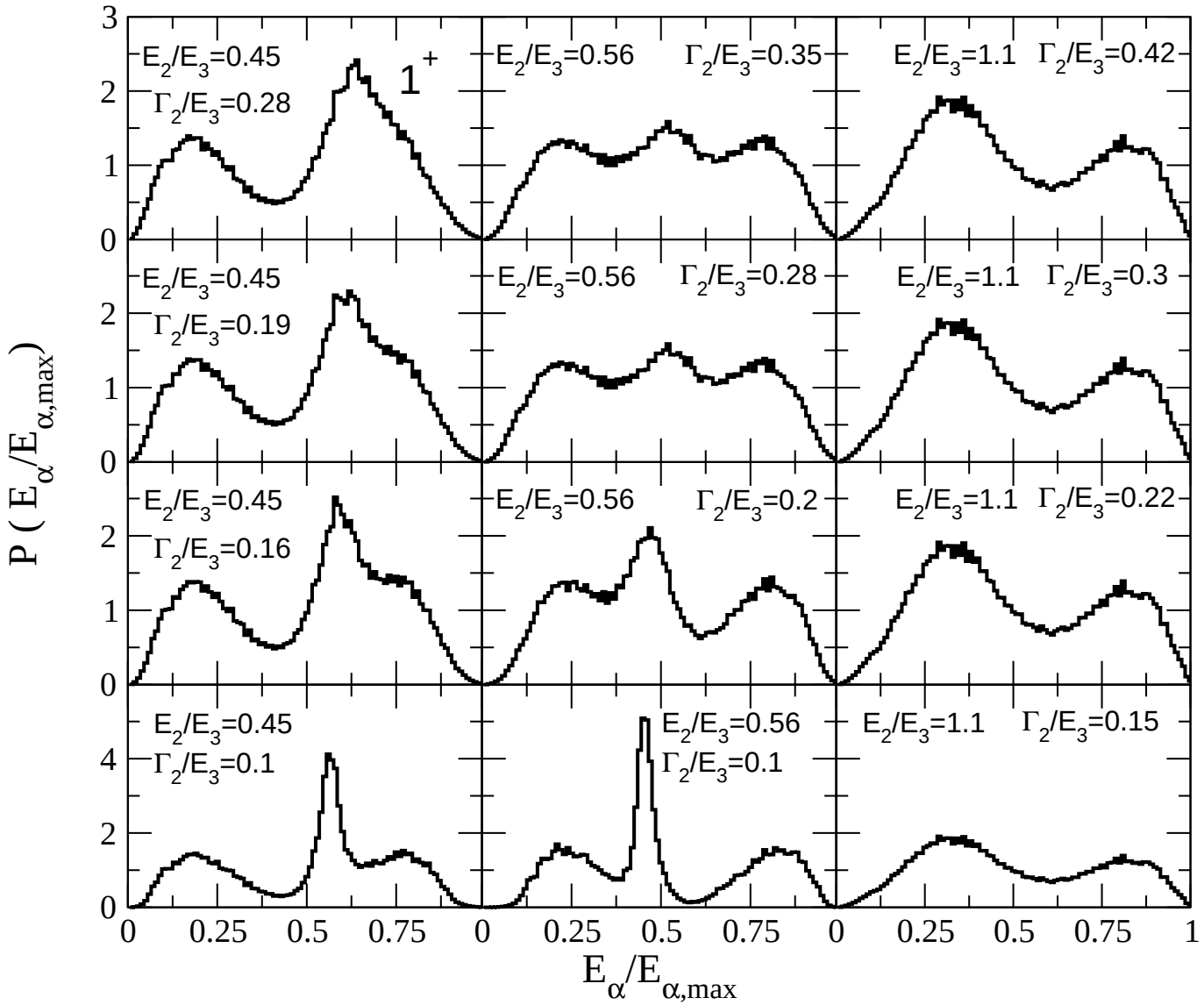

Figure 19: Single-alpha energy distributions from R-matrix analysis for decay into three α-particles of the 1^+ resonance in ^{12}C at an energy of $E_3 = 5.43$ MeV and a partial width of about 18 keV. The energies and widths of the intermediate 2^+ resonance in ^{8}Be are varied in the simulations as specified in the panels. The maximum energy $E_{\alpha,max} = 2E_3/3$. The symmetrization of the wavefunction is omitted.

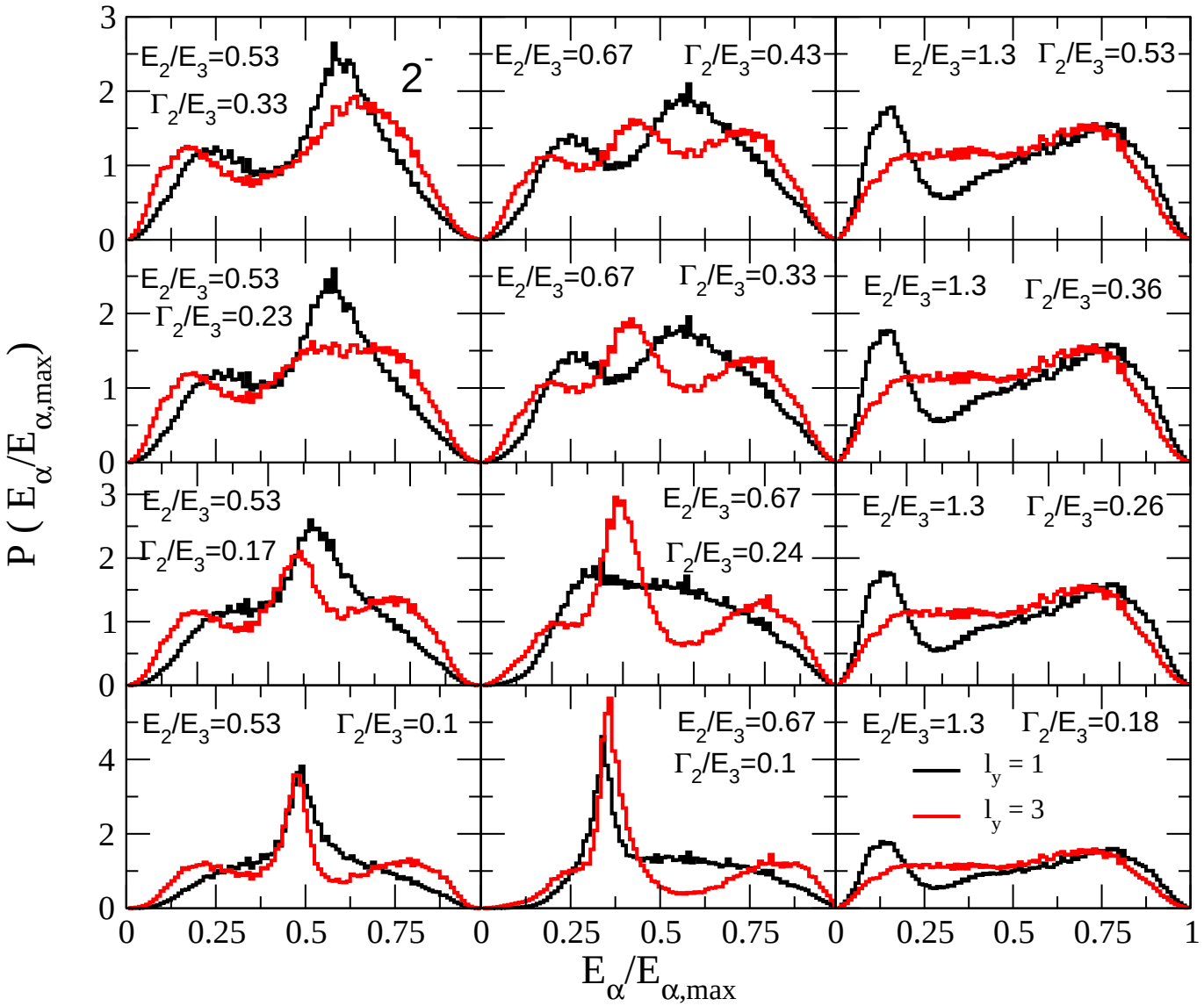

Figure 20: Single-alpha energy distributions from R-matrix analysis for decay into three α-particles of the 2^- resonance in ^{12}C at an energy of $E_3 = 4.55$ MeV. The energies and widths of the intermediate 2^+ resonance in ^{8}Be are given in the panels. The maximum energy $E_{\alpha,max} = 2E_3/3$. The red (solid) and black (dashed) curves are for, $\ell_y = 1, 3$, the two relative angular momenta between the first α-particle and ^{8}Be.

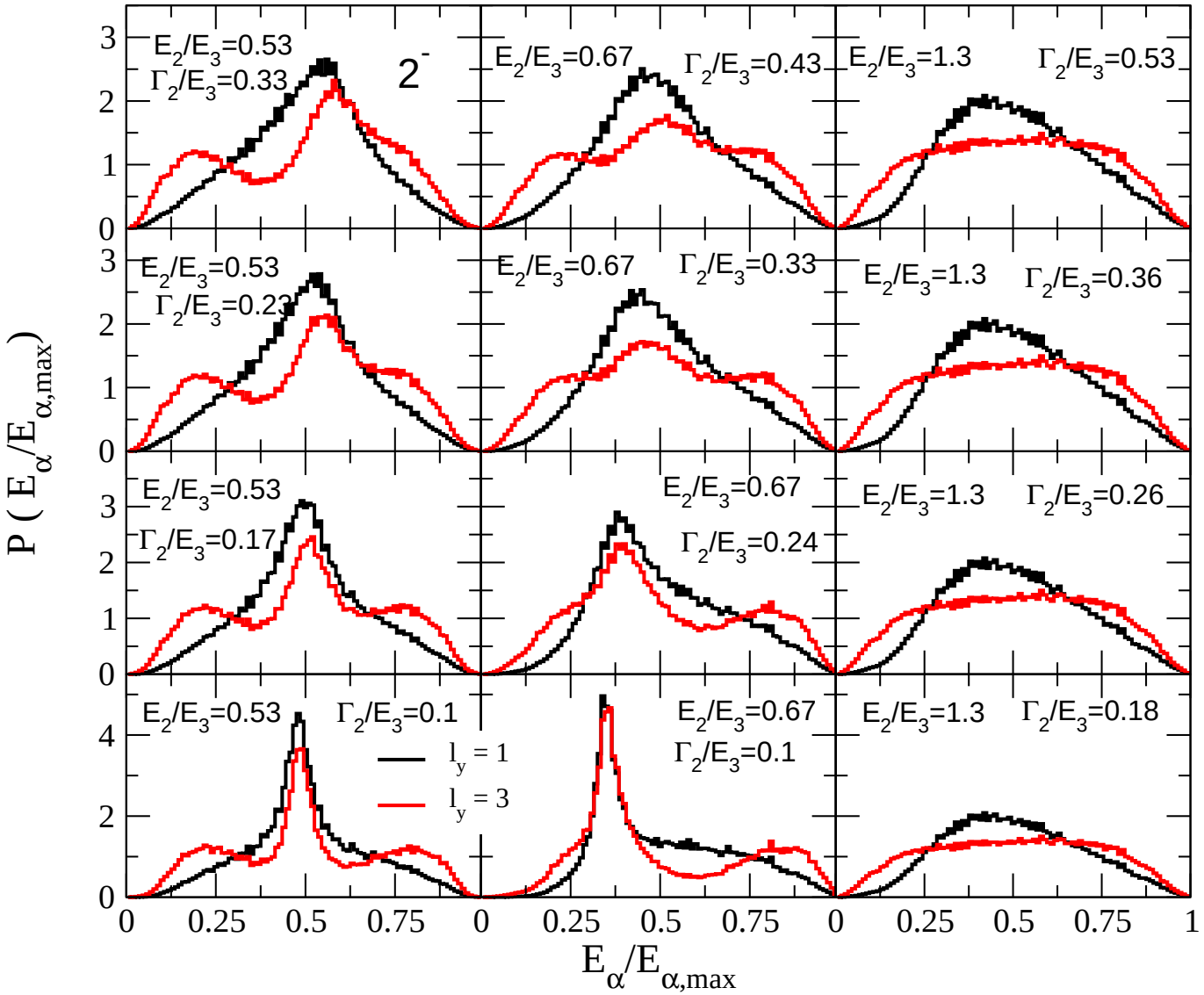

Figure 21: Single-alpha energy distributions from R-matrix analysis for decay into three α-particles of the 2^- resonance in ^{12}C at an energy of $E_3 = 4.55$ MeV. The energies and widths of the intermediate 2^+ resonance in ^{8}Be are given in the panels. The red (solid) and black (dashed) curves are for, $\ell_y = 1, 3$, the two possible relative angular momenta between the first α-particle and ^{8}Be. The symmetrization of the wavefunction is omitted.

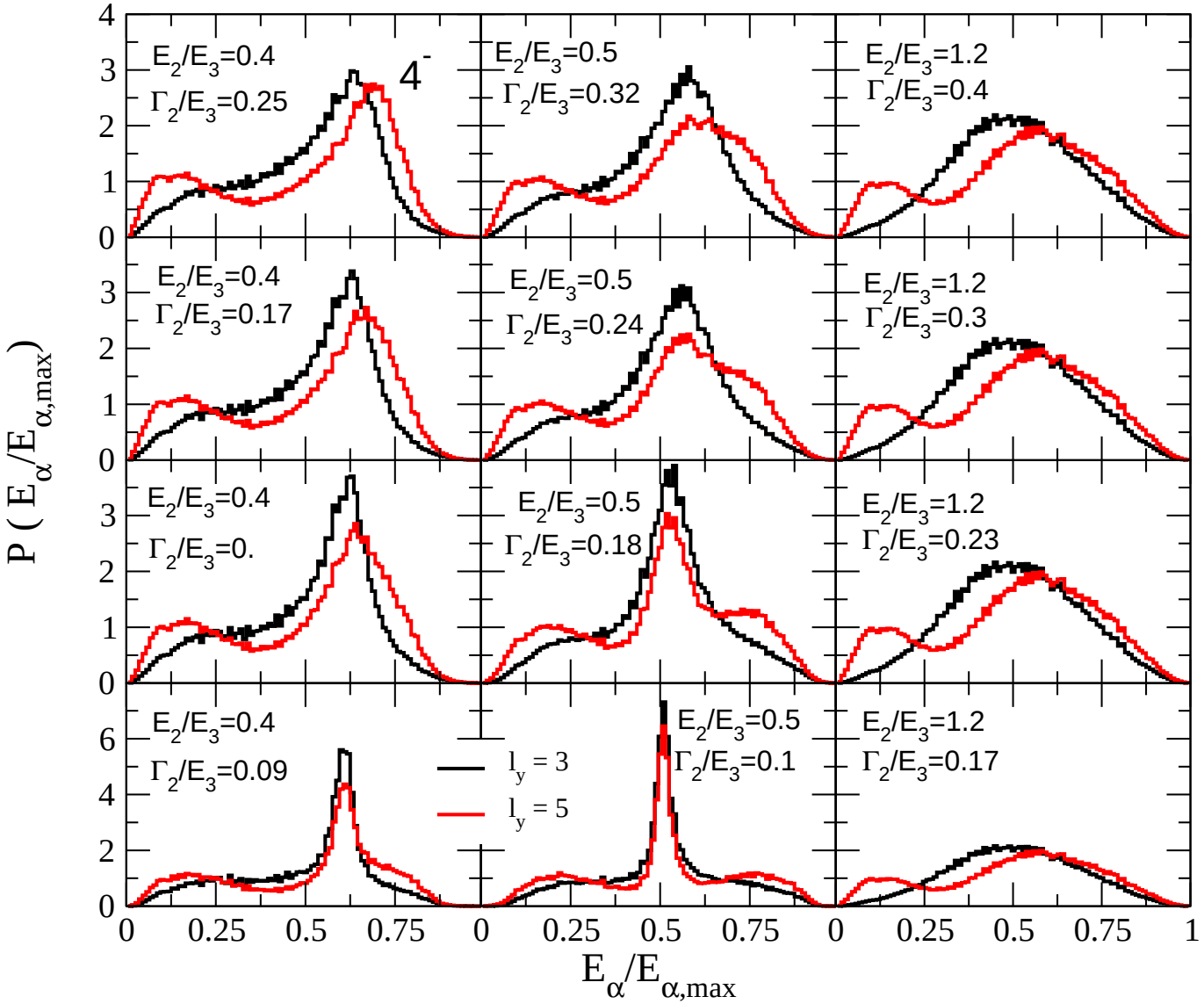

Figure 22: Single-alpha energy distributions from R-matrix analysis for decay into three α-particles of the 4^- resonance in ^{12}C at an energy of $E_3 = 6.08$ MeV and a partial width of about 375 keV. The energies and widths of the intermediate 2^+ resonance in ^{8}Be are given in the panels. The red (solid) and black (dashed) curves are for, $\ell_y = 3, 5$, the two possible relative angular momenta between the first α-particle and ^{8}Be.

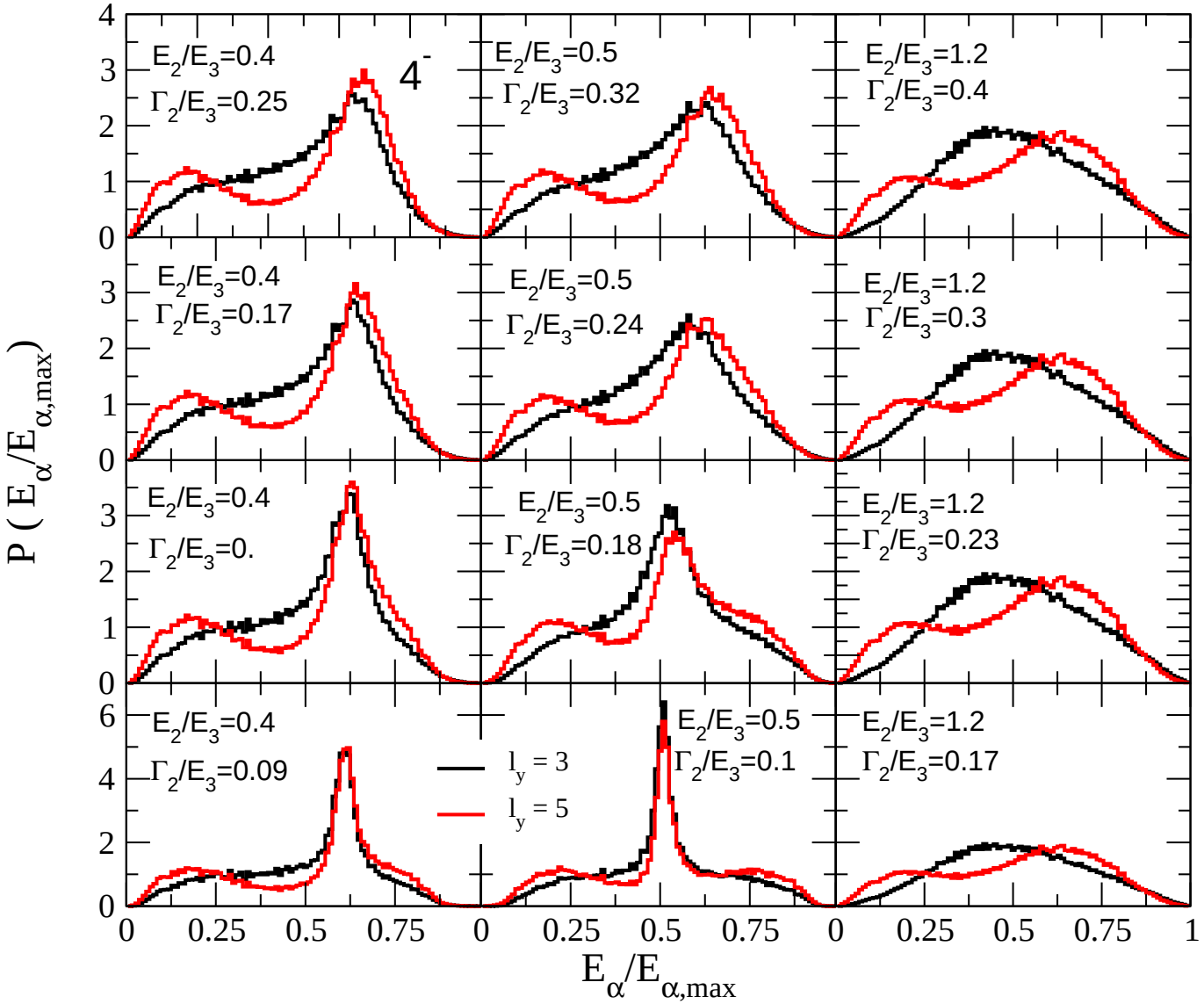

Figure 23: Single-alpha energy distributions from R-matrix analysis for three α-decay of the 4^- resonance in ^{12}C at an energy of $E_3 = 6.08$ MeV and a width of 375 keV. The energies and widths of the intermediate 2^+ resonance in ^{8}Be are given in the panels. The red (solid) and black (dashed) curves are for, $\ell_y = 3, 5$, the two relative angular momenta between the first α-particle and ^{8}Be. The symmetrization of the wavefunction is omitted.

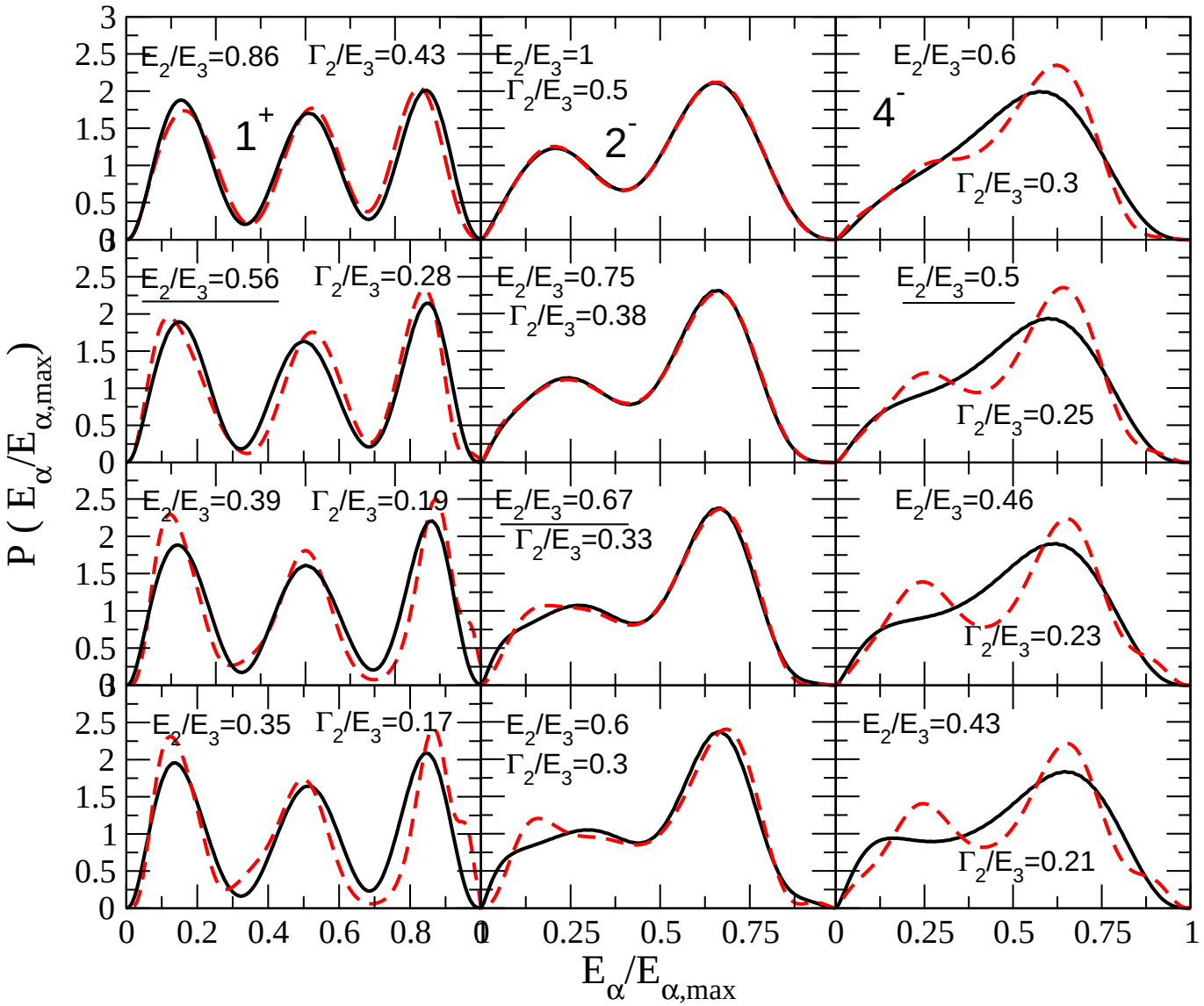

Figure 24: Single-alpha energy distributions from full computation for direct decay into three α-particles of the 1^+, 2^-, 4^- resonances in ^{12}C at the measured energies of $E_3 = 5.43, 6.08, 4.55$ MeV. These energies are varied by change of the strength of the three-body potential. The relative energies and widths of the intermediate 2^+ resonance in ^{8}Be are given in the panels. The full (black) and dashed (red) are for rotation angle $\theta = 0.25$ and 0.1.

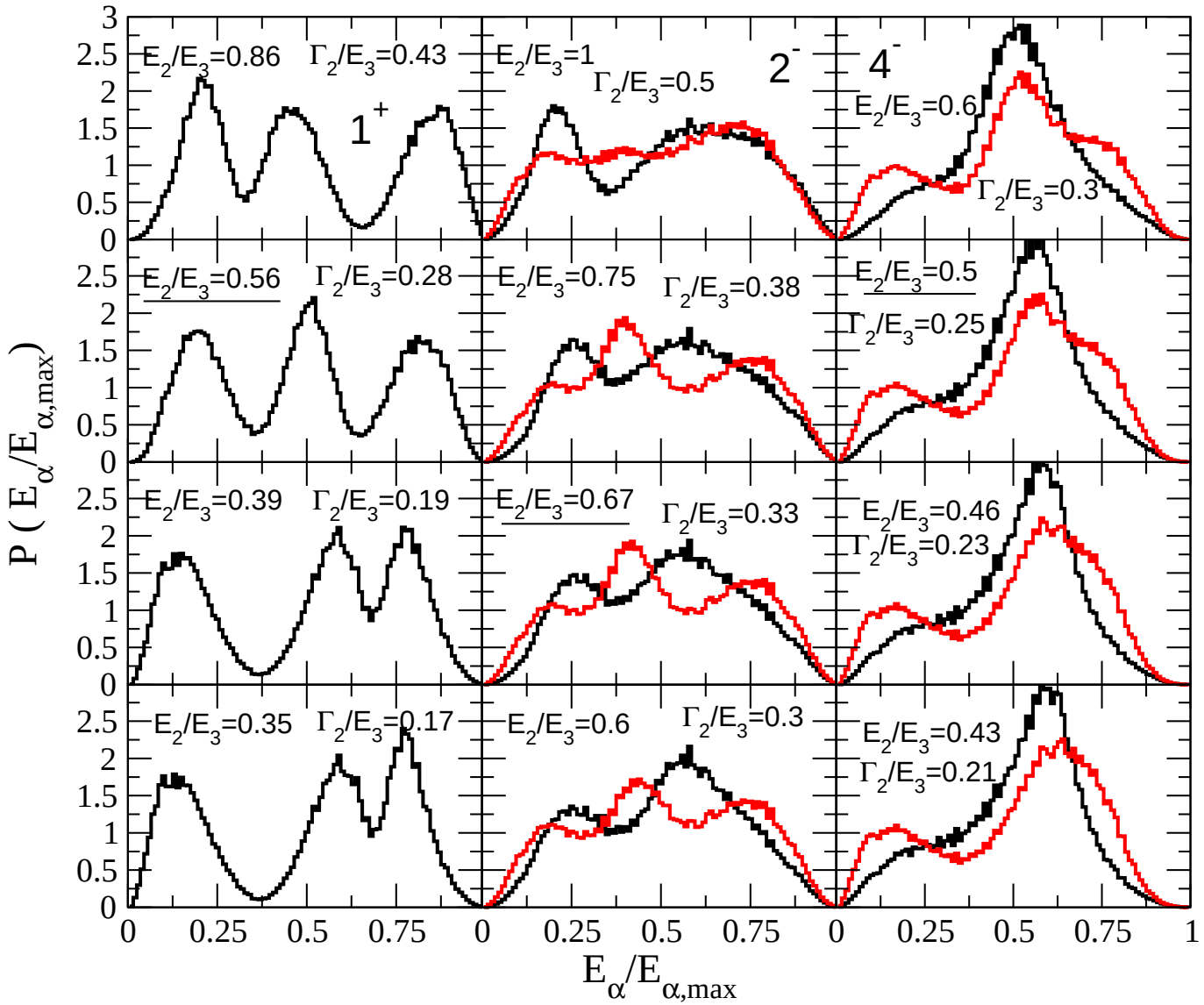

Figure 25: Single-alpha energy distributions from R-matrix computation for decay into three α-particles of the 1^+, 2^-, 4^- resonances in ^{12}C at the measured energies of $E_3 = 5.43, 6.08, 4.55$ MeV, respectively. The parameters shown in the panels are the same as in fig. 24. The full (black) and dashed (red) are for $\ell_y = 1, 3$ and $\ell_y = 3, 5$ respectively for the 2^- and 4^- resonances.

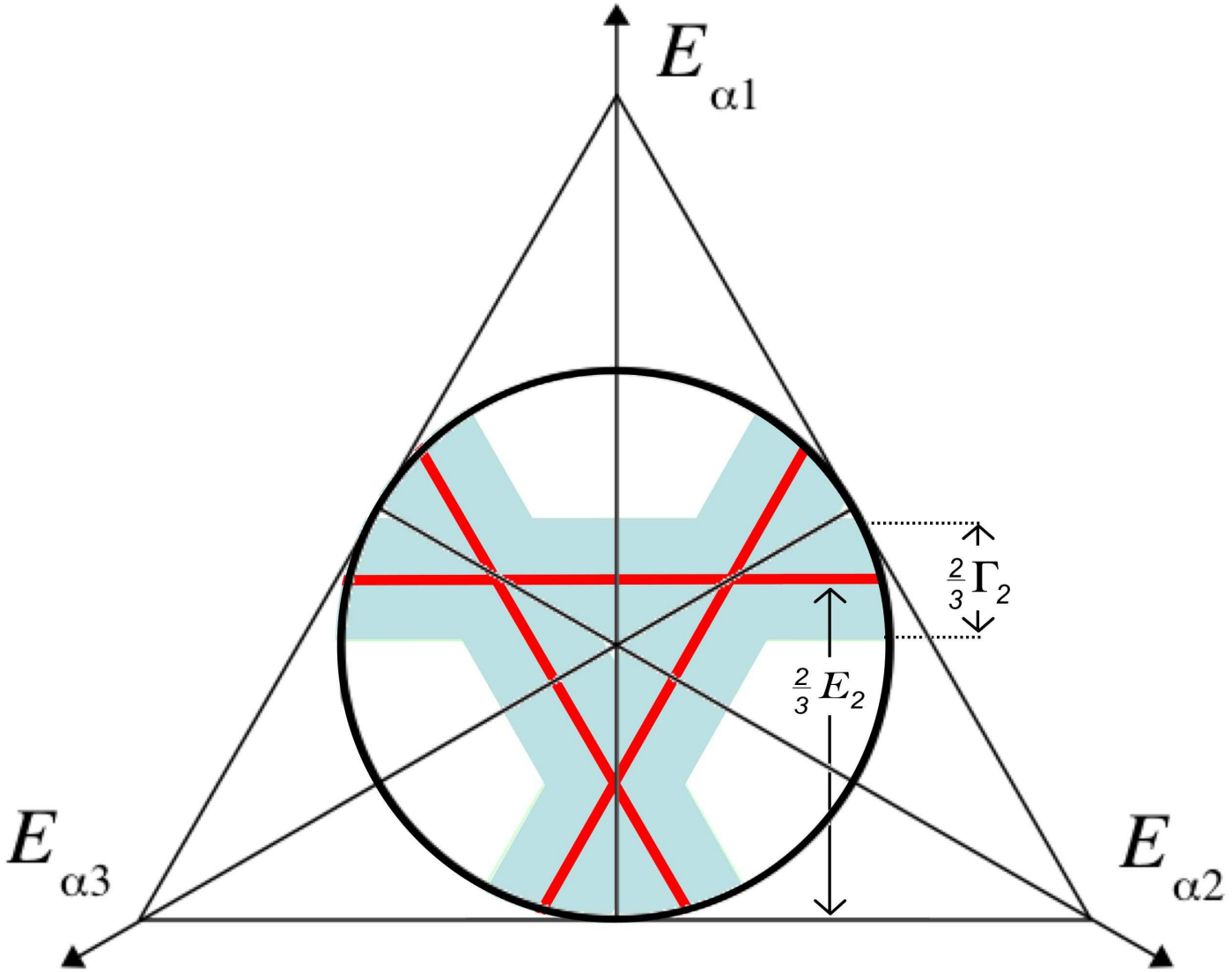

Figure 26: Density structures of the Dalitz plot for sequential decays. The inscribed circle marks the boundary of the kinematically allowed region.

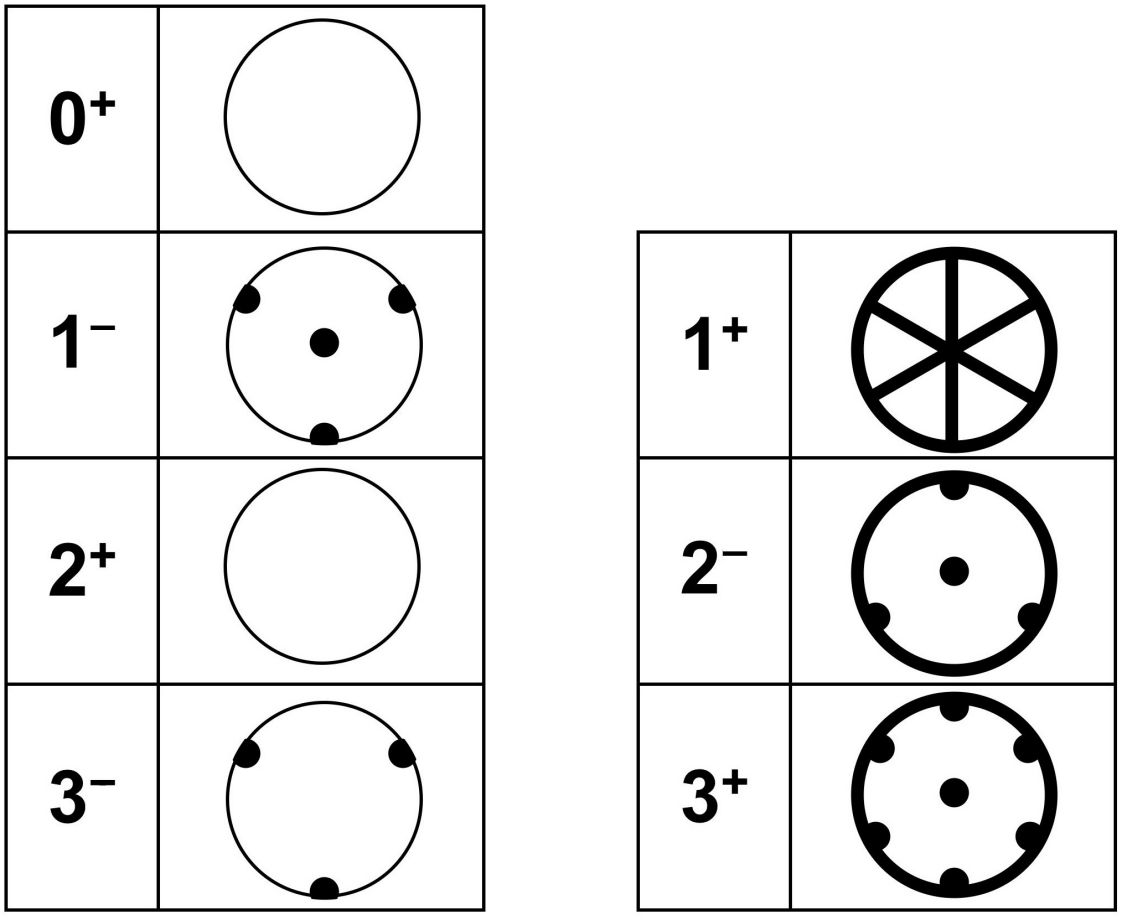

Figure 27: Regions of the 3α Dalitz plot where the density must vanish are shown in black. The vanishing is of higher order where the black lines and dots overlap. The pattern for a spin $J+2n$ ($n = 1, 2, 3, \ldots$) is identical to the pattern for spin J (provided $J \geq 2$) except that the vanishing at the center is not required for spins $J \geq 4$.

Nodes in Dalitz plots

Forced by parity and angular momentum conservation

The momentum distributions are essentially given by:

$\left|\Psi\left(\rho_{max}, \Omega_k\right)\right|^2$, coordinate wavefunction

$\Omega_k = \left\{\Omega_{kx}, \Omega_{ky}, \alpha_k\right\}$, momentum coordinates

Unavoidable nodes from parity and angular momentum structure

Also other points of zero probability can be found in $\left|\Psi\left(\rho_{max}, \Omega_k\right)\right|^2$

They are nodes in the coordinate wavefunction at large distance ρ_{max}

They may differ from those at small distance due to dynamic evolution

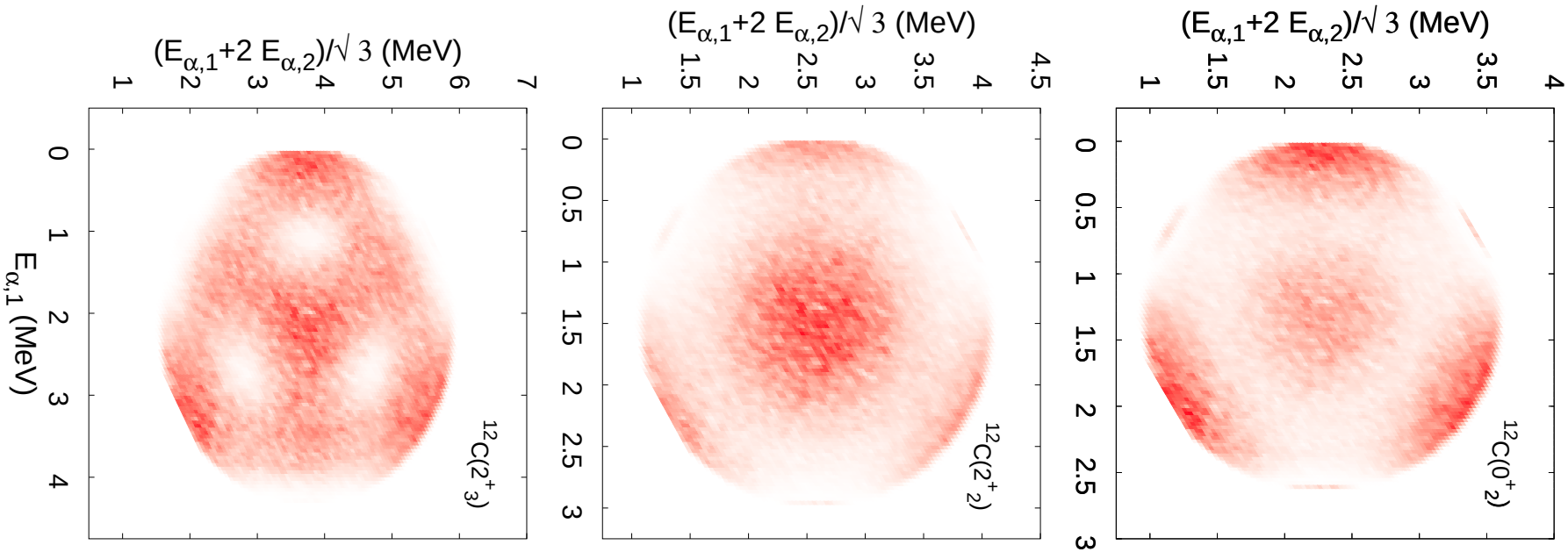

Figure 28: Dalitz plot of the α-particle energy distribution for the $(0_2^+, 2_2^+, 2_3^+)$-resonances in ^{12}C at (4.3, 4.48, 6.49) MeV above the 3α threshold at an excitation energy larger by 7.275 MeV.

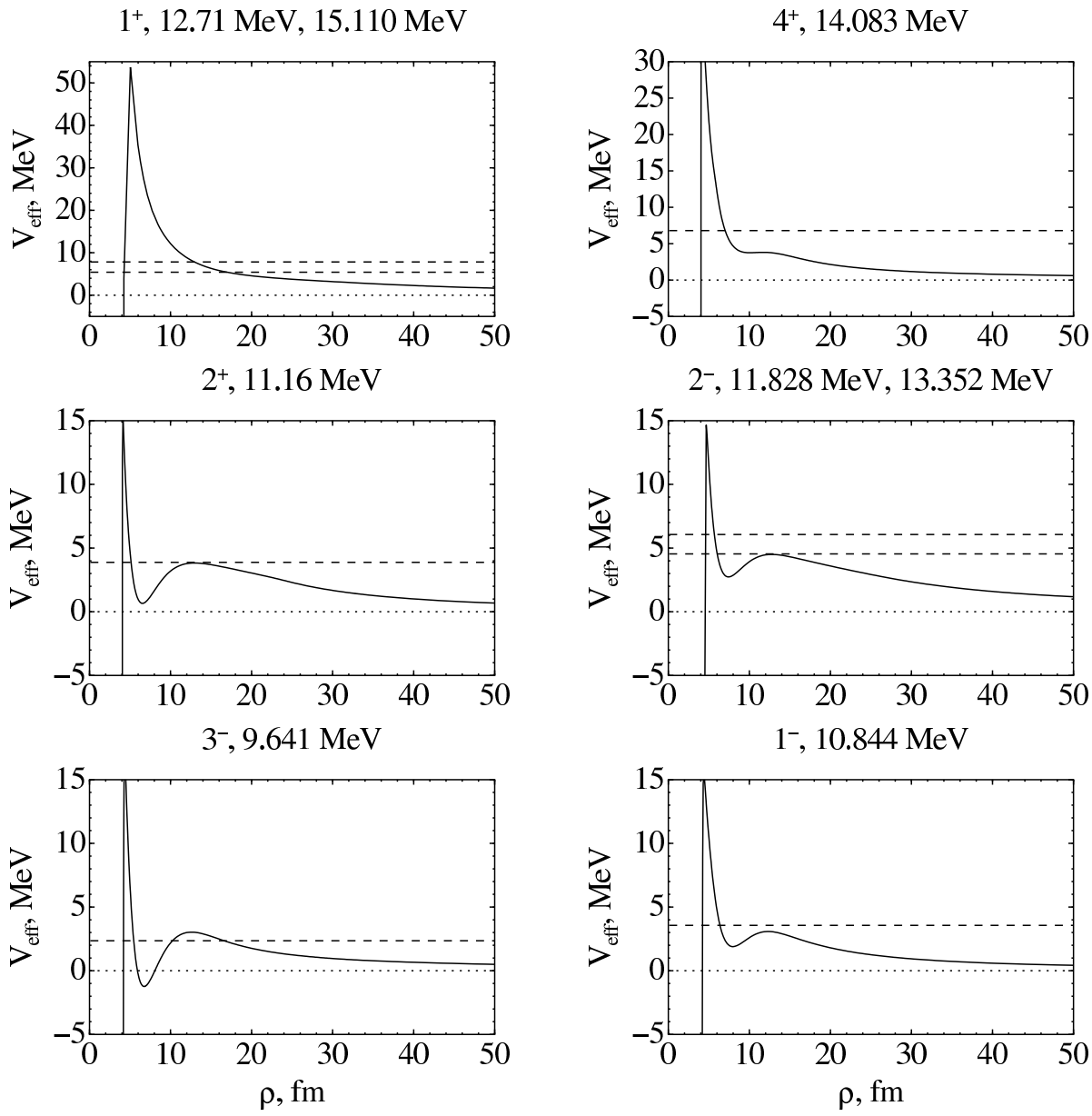

Figure 29: The computed lowest adiabatic potential as function of hyperradius for a number of resonances of ^{12}C (α+α+α). The horizontal lines mark the resonance energies measured above the three-body threshold. The corresponding excitation energies are given above each of the panels [42].

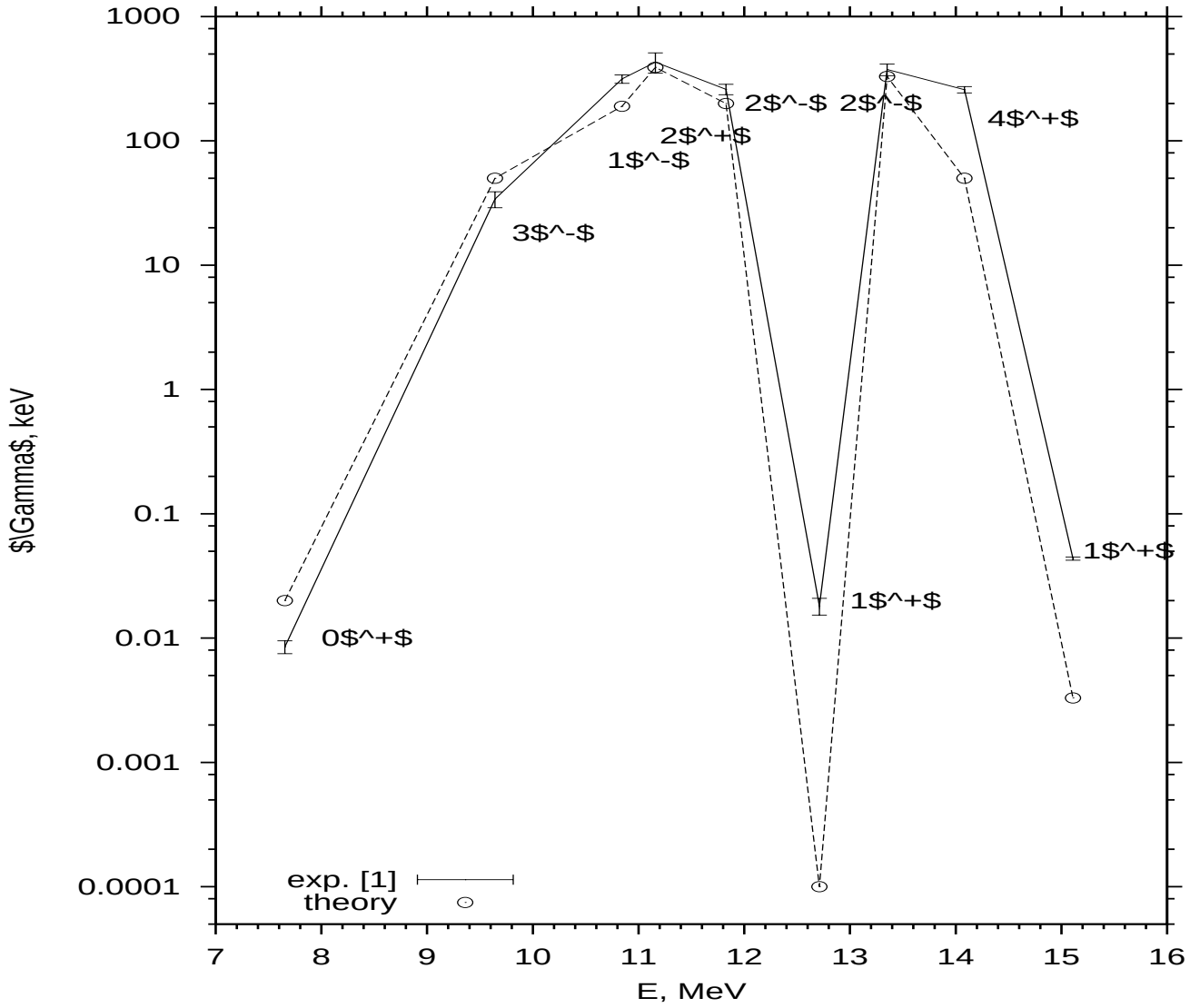

Figure 30: The computed widths compared to the measured values for different resonances of ^{12}C with excitation energy E [42]. The WKB approximation is used for tunneling through the lowest adiabatic potential where the inner turning point is fixed to a hyperradius of $\rho = 4$ fm.

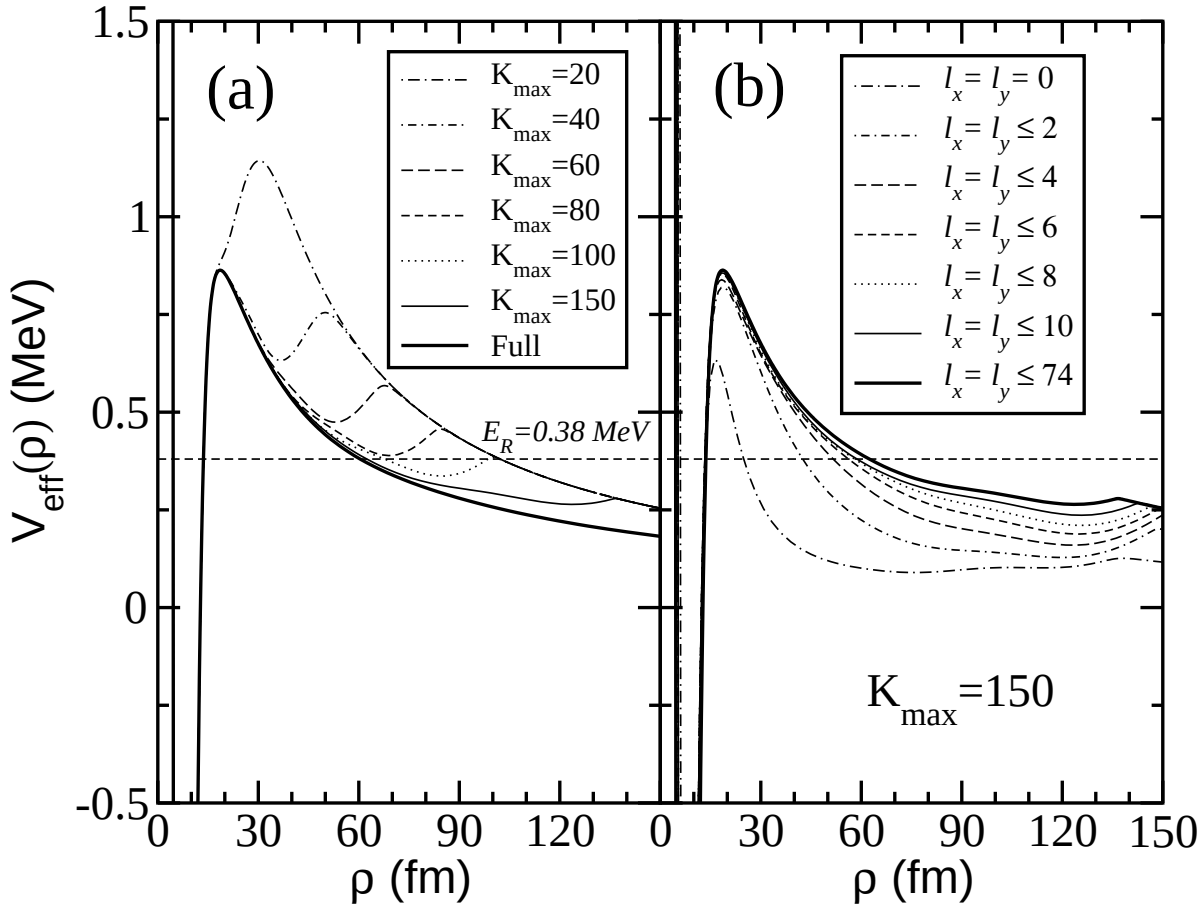

Figure 31: The dominating effective adiabatic potential for the lowest 0^+ resonance in ^{12}C (α+α+α) for (a) different values of K_{max} and (b) different values of partial waves in the expansion in terms of HH. The dashed straight line indicates the energy of the resonance. In (a) all the the possible values of ℓ_x and ℓ_y consistent with K_{max} have been included. The curve called "full" includes $\ell_x = \ell_y$ up to 12 only and K_{max}=150, but with K_{max} increased up to 500 for some of the components. In (b) K_{max} is taken equal to 150.

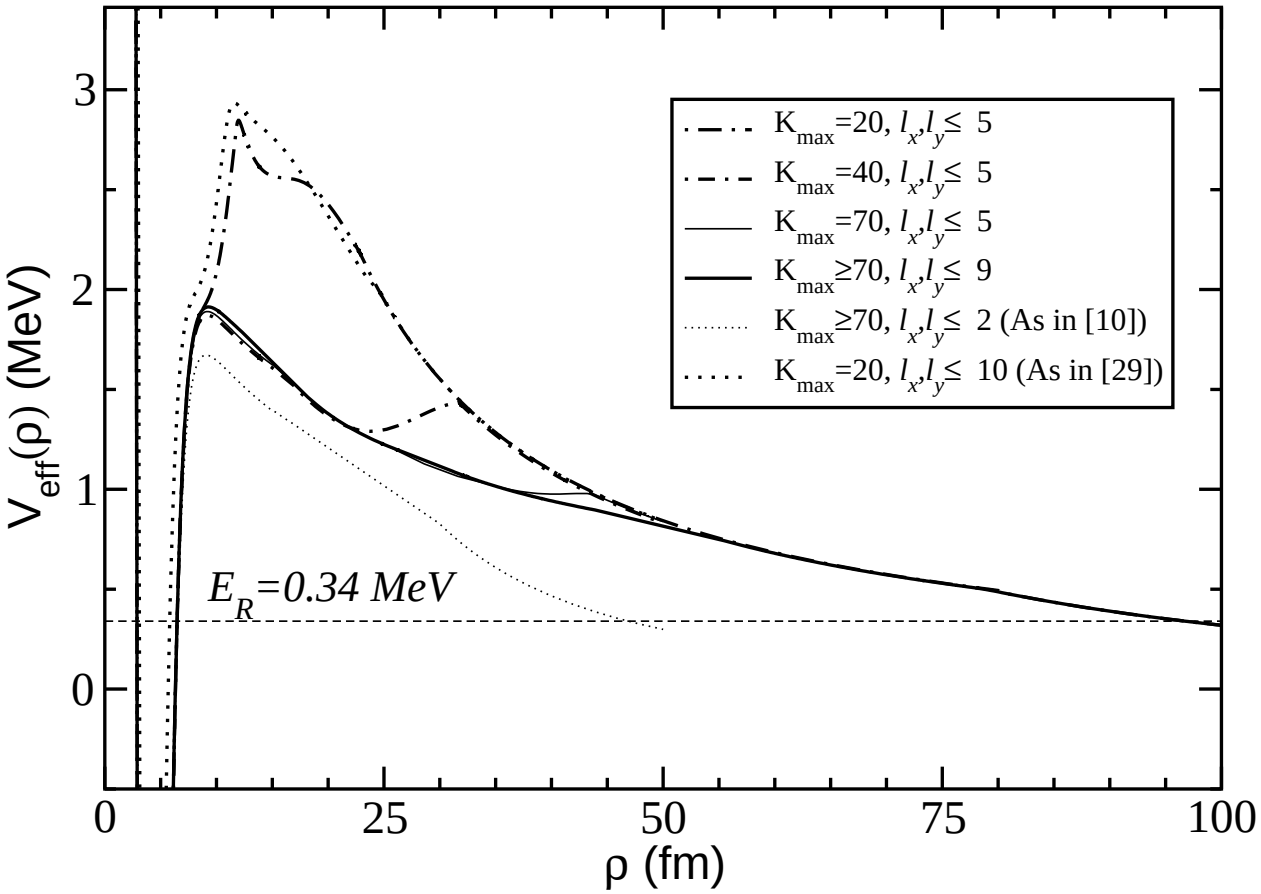

Figure 32: Lowest adiabatic effective potential for the $3/2^-$ resonance in ^{17}Ne. Except for the last curve (thick-dot), the p-^{15}O interaction is the one described in [44]. The different curves correspond to calculations with different values of K_{max} and relative two-body angular momenta. The thin-dotted curve corresponds to the calculation presented in [44]. In the last (thick-dotted) curve, the p-^{15}O potential and K_{max} value of ref.[45] have been used. The dashed straight line indicates the resonance energy of 0.34 MeV.

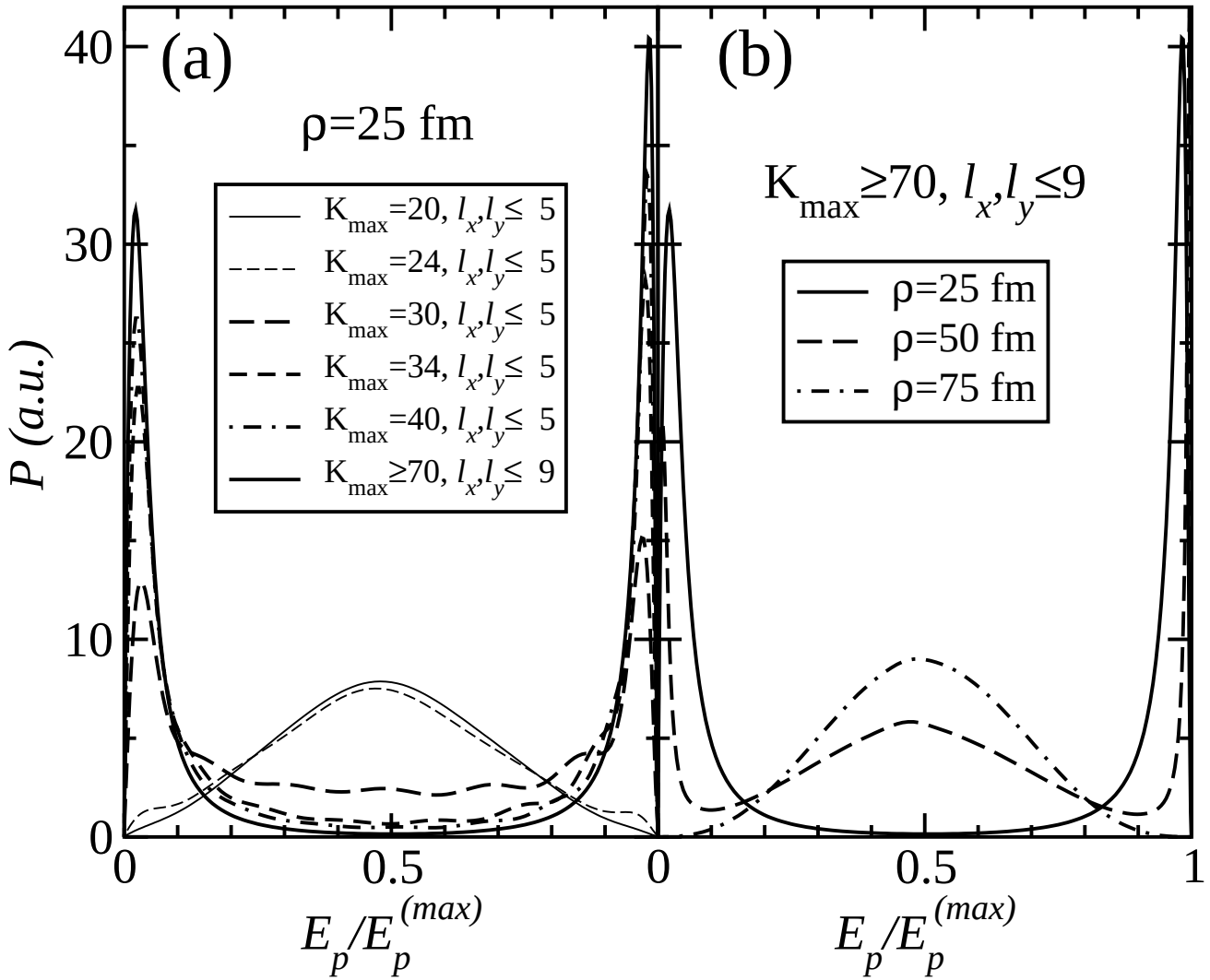

Figure 33: Proton energy distributions for the $3/2^-$ resonance in ^{17}Ne where the maximum allowed emission energy is used as unit. The left part is for ρ=25 fm for different values of K_{max}. The right part is for a very large basis for increasing hyperradii. Only the lowest adiabatic effective potential is used.

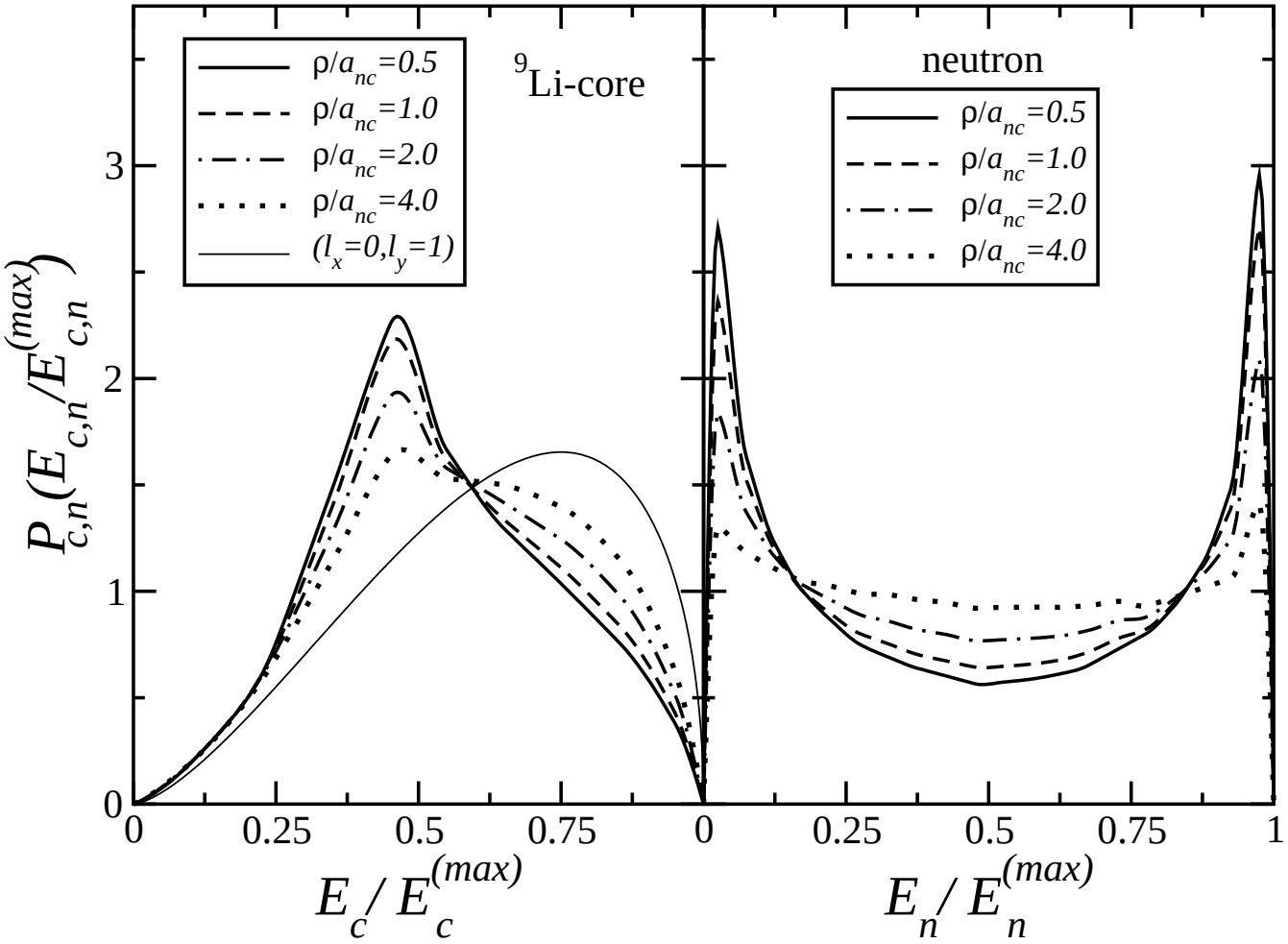

Figure 34: The neutron and core energy distributions P_j from decay of ^{11}Li(1^-) for different ρ as function of the particle energies E_n and E_c in units of their maxium values. The neutron-core scattering length is $a_{nc} = 48.2$ fm and only components with $(\ell_x^{(nc)}, \ell_y^{(nc)}) = (0, 1)$ are included. The free solutions are shown as thin dashed and dot-dashed curves.

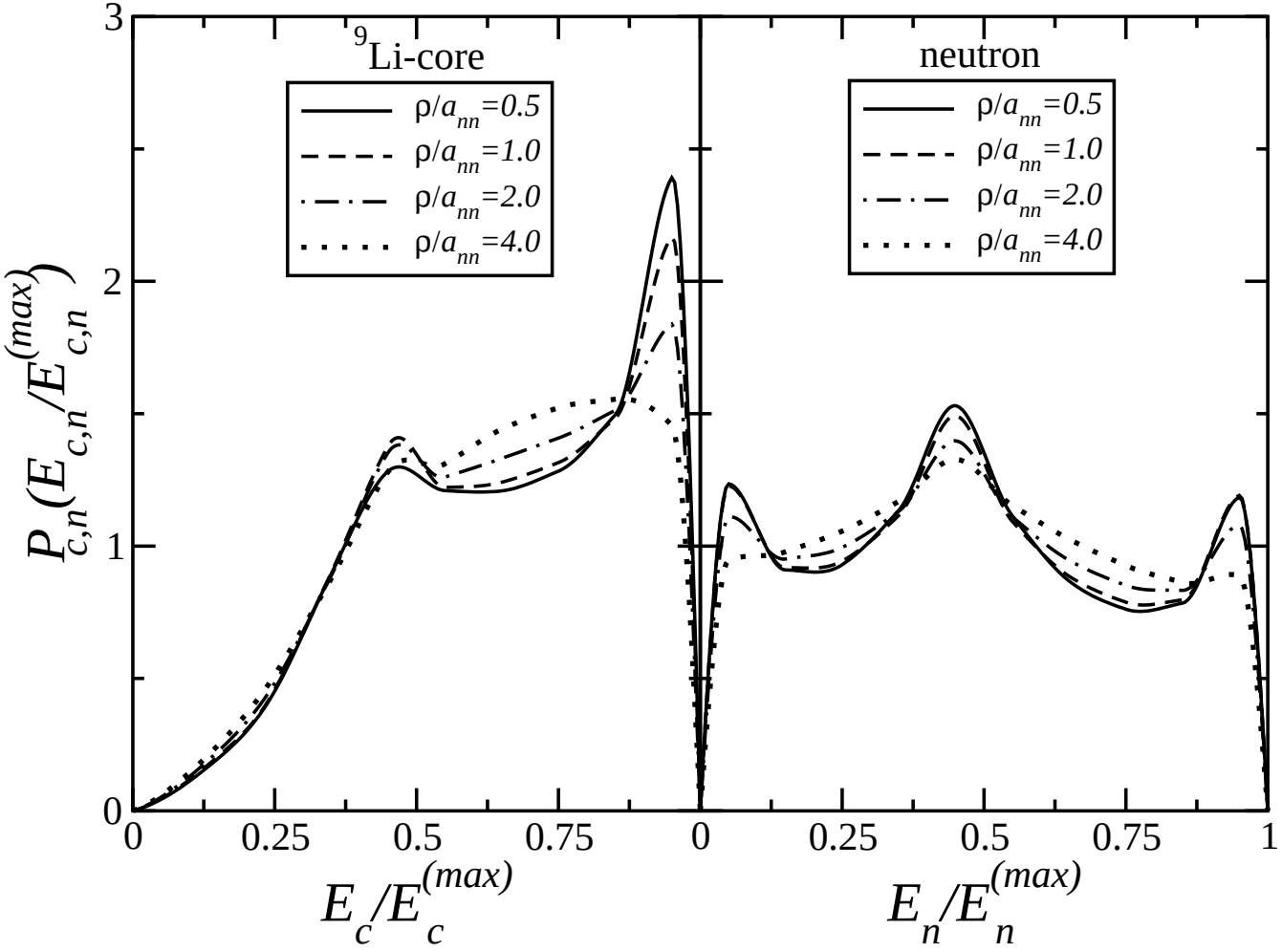

Figure 35: The same as fig. 34 for neutron-neutron and neutron-core scattering lengths $a_{nn} = a_{nc} = 48.2$ fm with the three components $(\ell_x^{(nn)}, \ell_y^{(nn)}) = (0,1)$, $(\ell_x^{(nc)}, \ell_y^{(nc)}) = (0,1)$.

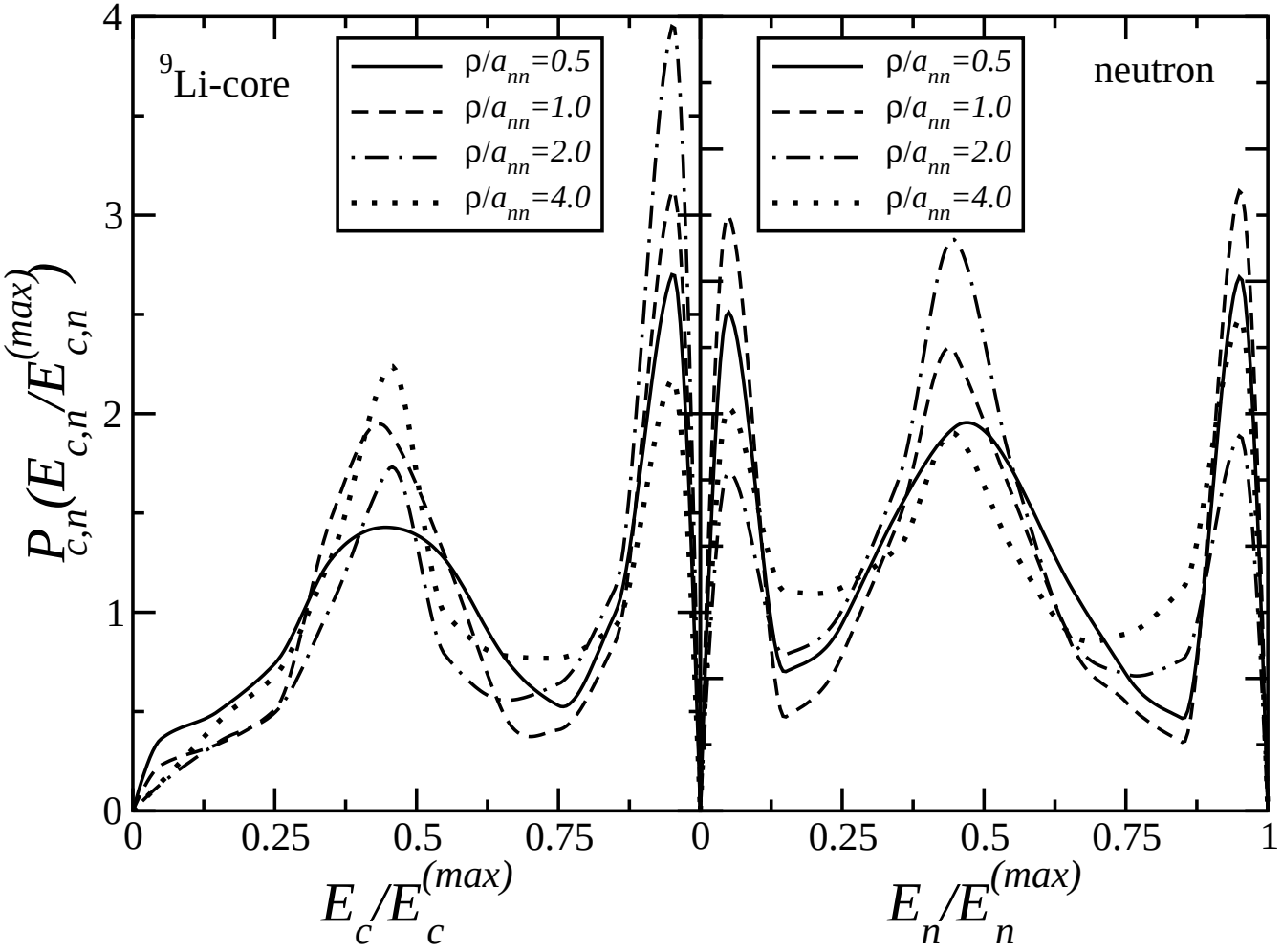

Figure 36: The same as fig. 34 for realistic interactions, $a_{nn} = a_{nc} \approx 20$ fm, $R_{eff} \approx 5$ fm [43]. All contributing partial waves and adiabatic potentials are included.

Summary and Conclusions

1. Three-body decays; a generalization of α-emission
2. Small distances cover the many-body character
3. Large distances reflect the three-body observables after decay
4. Dynamic evolution of resonance structure from small to large distances
5. Partial decay widths can be estimated;
   preformation factor or spectroscopic factors are necessary
6. Direct and sequential, not quantum mechanical distinguishable
   R-matrix analyses indicate limits when they are distinguishable
7. Direct is largely determined by Coulomb and centrifugal barriers;
   two-body interactions provide the correct small-distance structure
8. Sequential via two-body substructures determined by pair interactions;
   widths and momentum distributions depend sensitively
9. Method must describe different substructure;
   coherent two-body substructures, a la Efimov
10. Angular momentum and parity, fermion or boson symmetry are crucial
11. Dalitz plots reveal details, experimental and theory comparison
12. ^{12}C, ^{9}Be, ^{6}Be, agree with measurements, Efimov effect in ^{11}Li

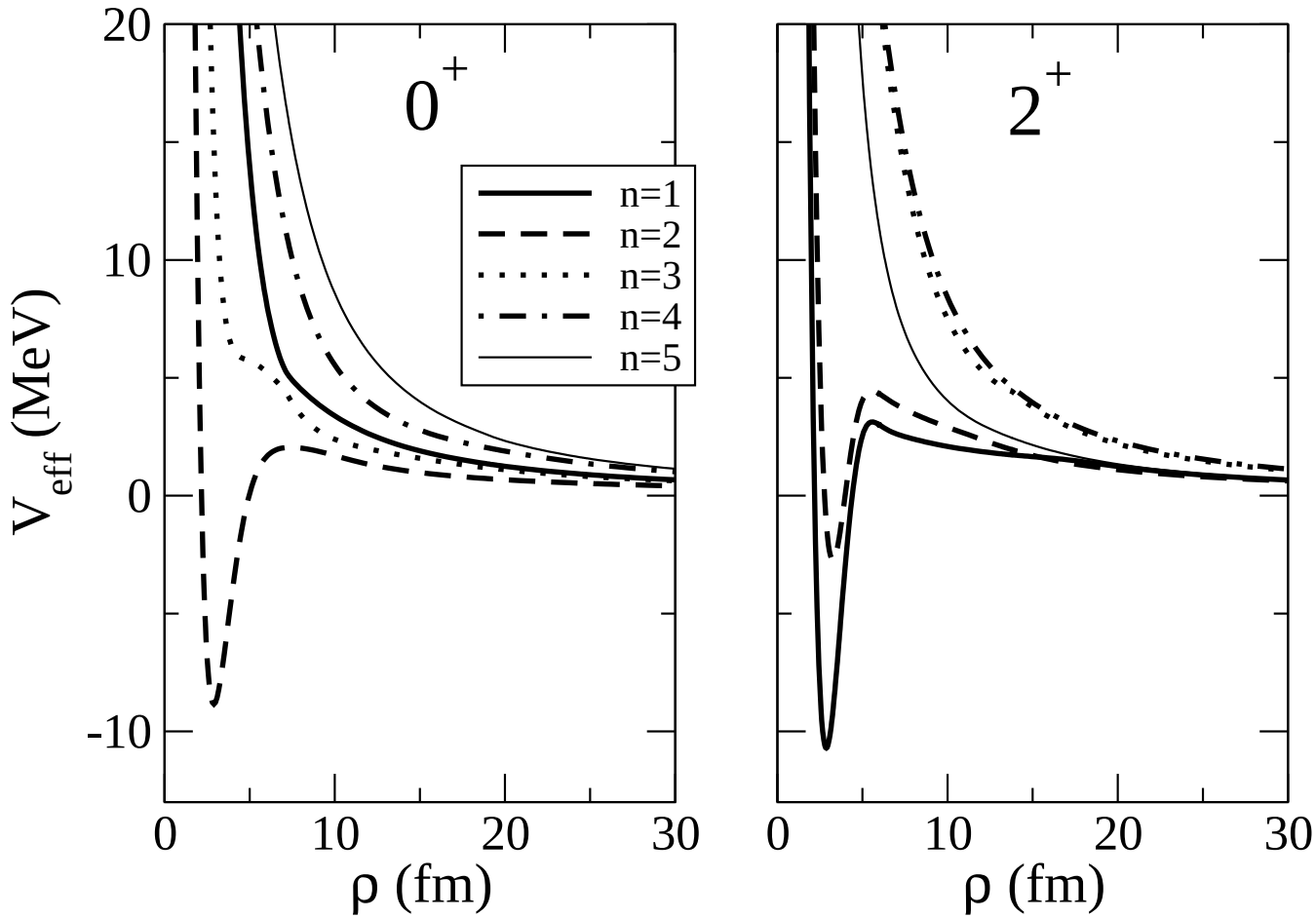

Figure 37: The real parts of the five lowest adiabatic effective potentials, including 3-body potential, as a function of the hyperradius for the 0^+ (left) and 2^+ (right) resonances of ^{6}Be.

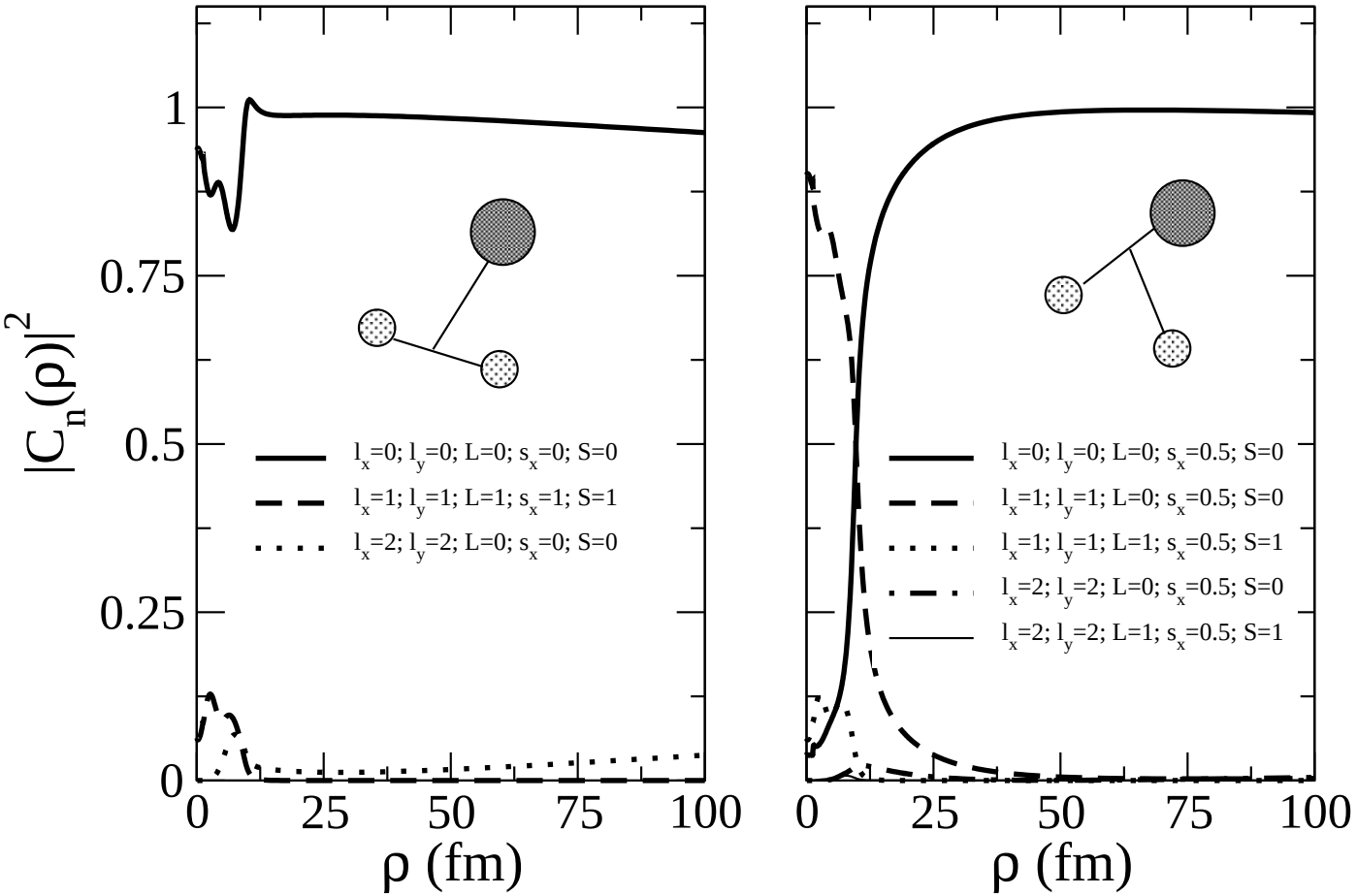

Figure 38: The partial-wave decomposition of the ^{6}Be(0^+) resonance as a function of the hyperradius for the dominating adiabatic component.

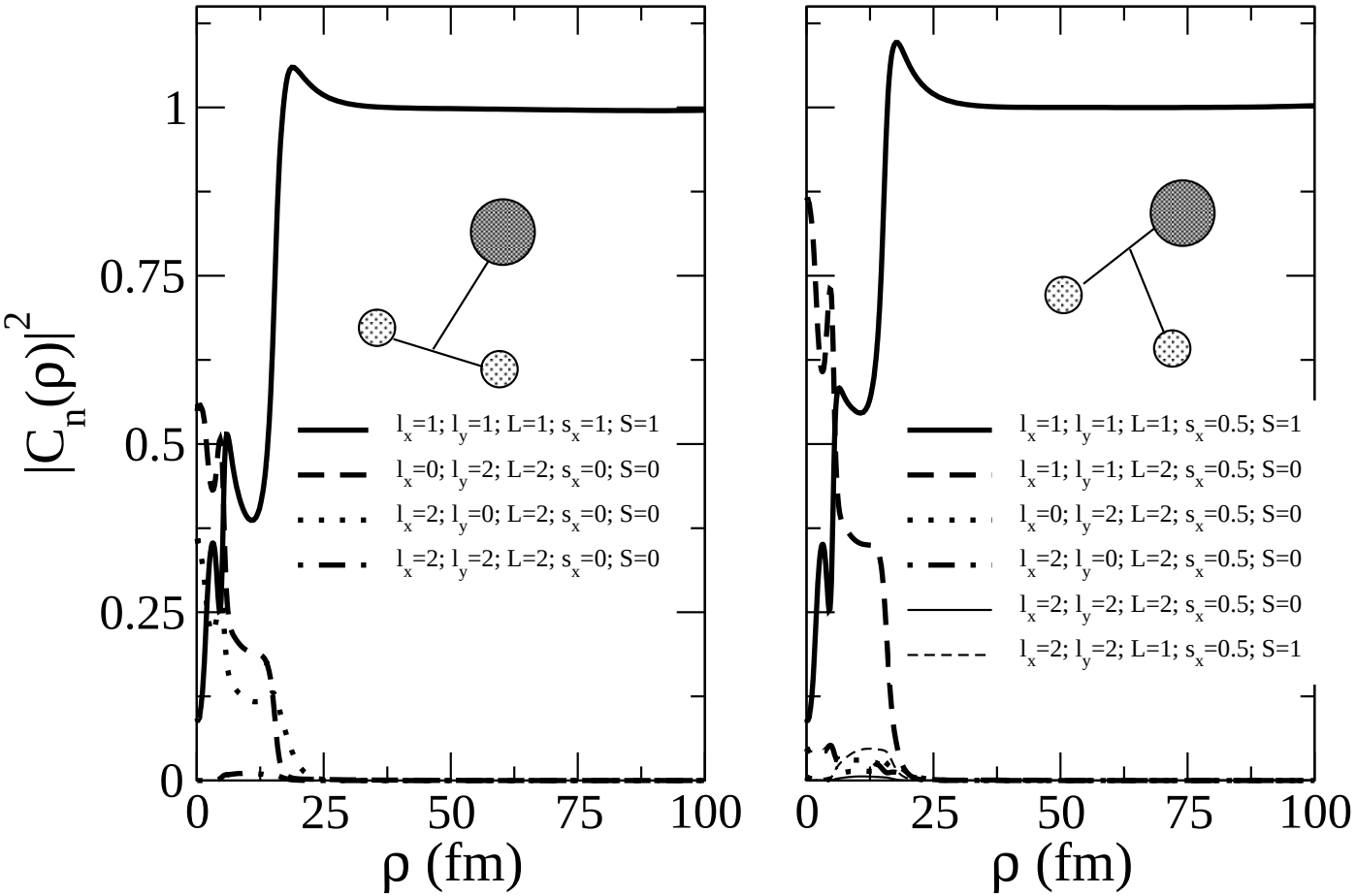

Figure 39: The partial-wave decomposition of the ^{6}Be(2^+) resonance as a function of the hyperradius for the dominating adiabatic component.

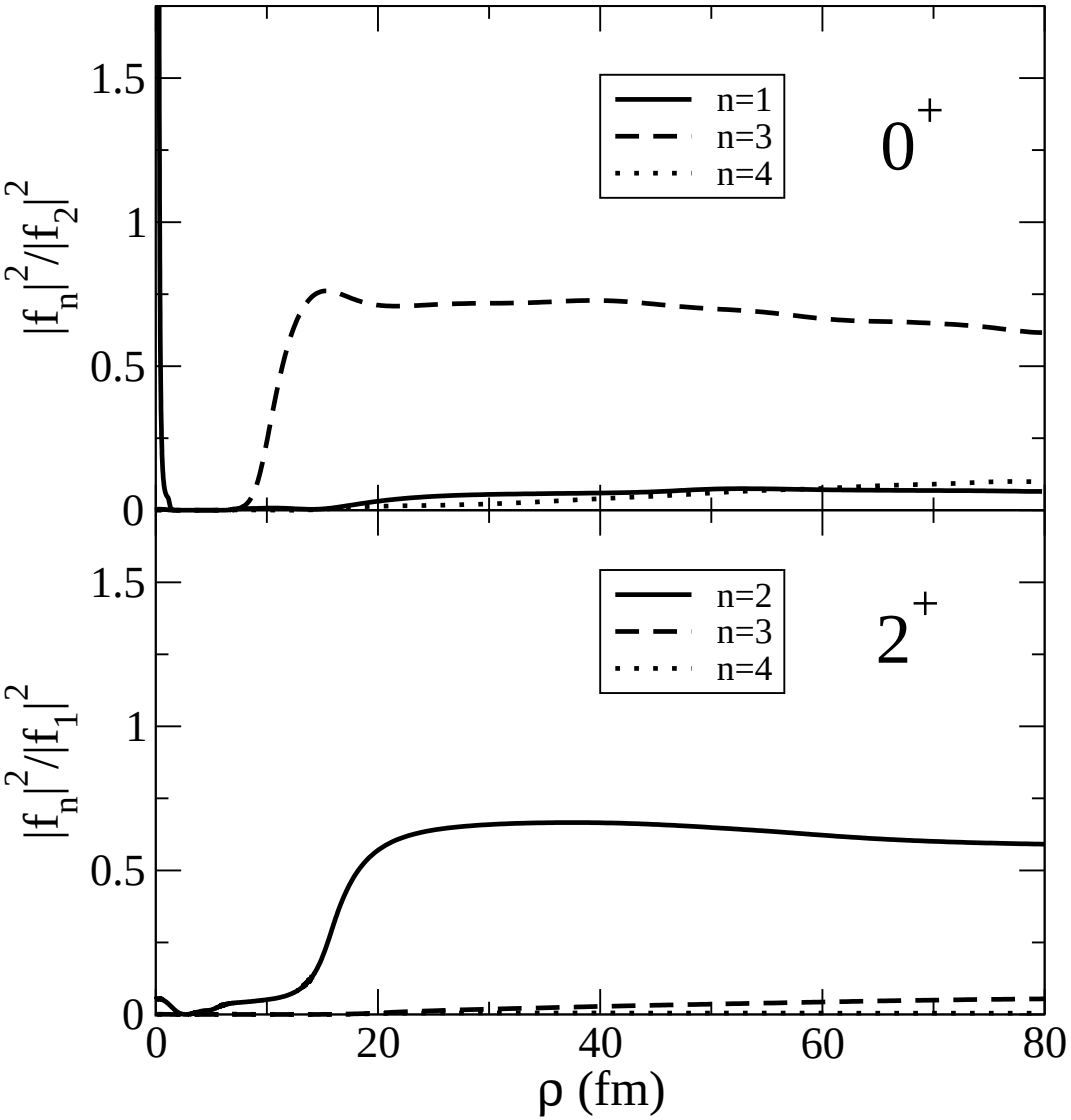

Figure 40: Ratios of the different adiabatic components of the radial wave function for both 0^+ (up) and 2^+ (down) resonances of ^{6}Be. The denominator is in both cases the component that gives most of the contribution.

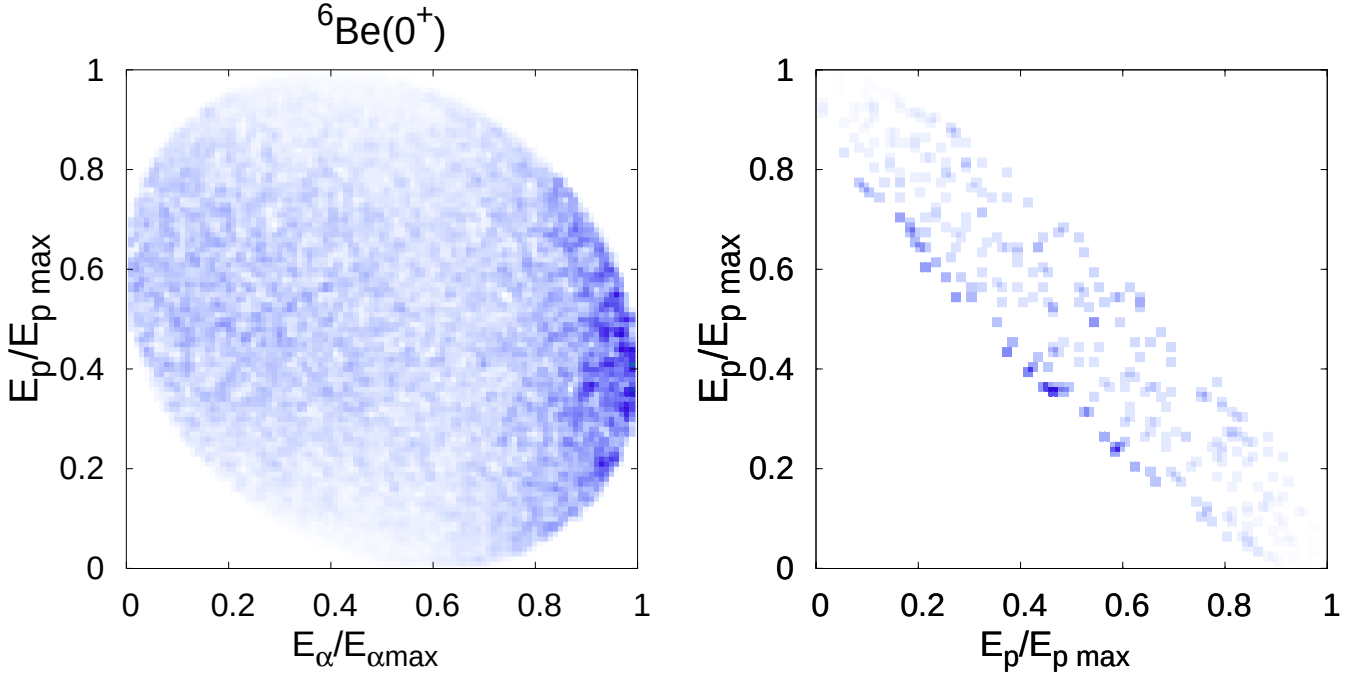

Figure 41: Dalitz plots for the probability of finding an α particle and a proton with a given energy (left) or the two protons (right) for the 0^+ resonance of ^{6}Be.

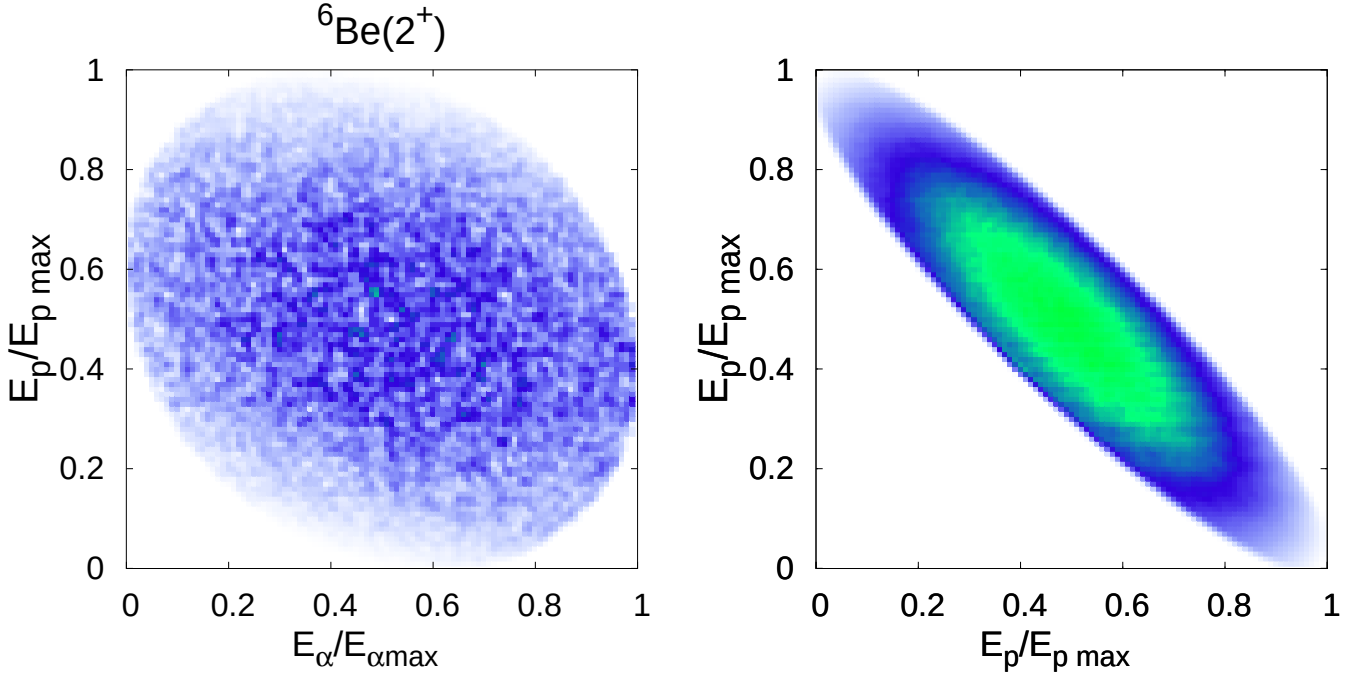

Figure 42: Dalitz plots for the probability of finding an α particle and a proton with a given energy (left) or the two protons (right) for the 2^+ resonance of ^{6}Be.

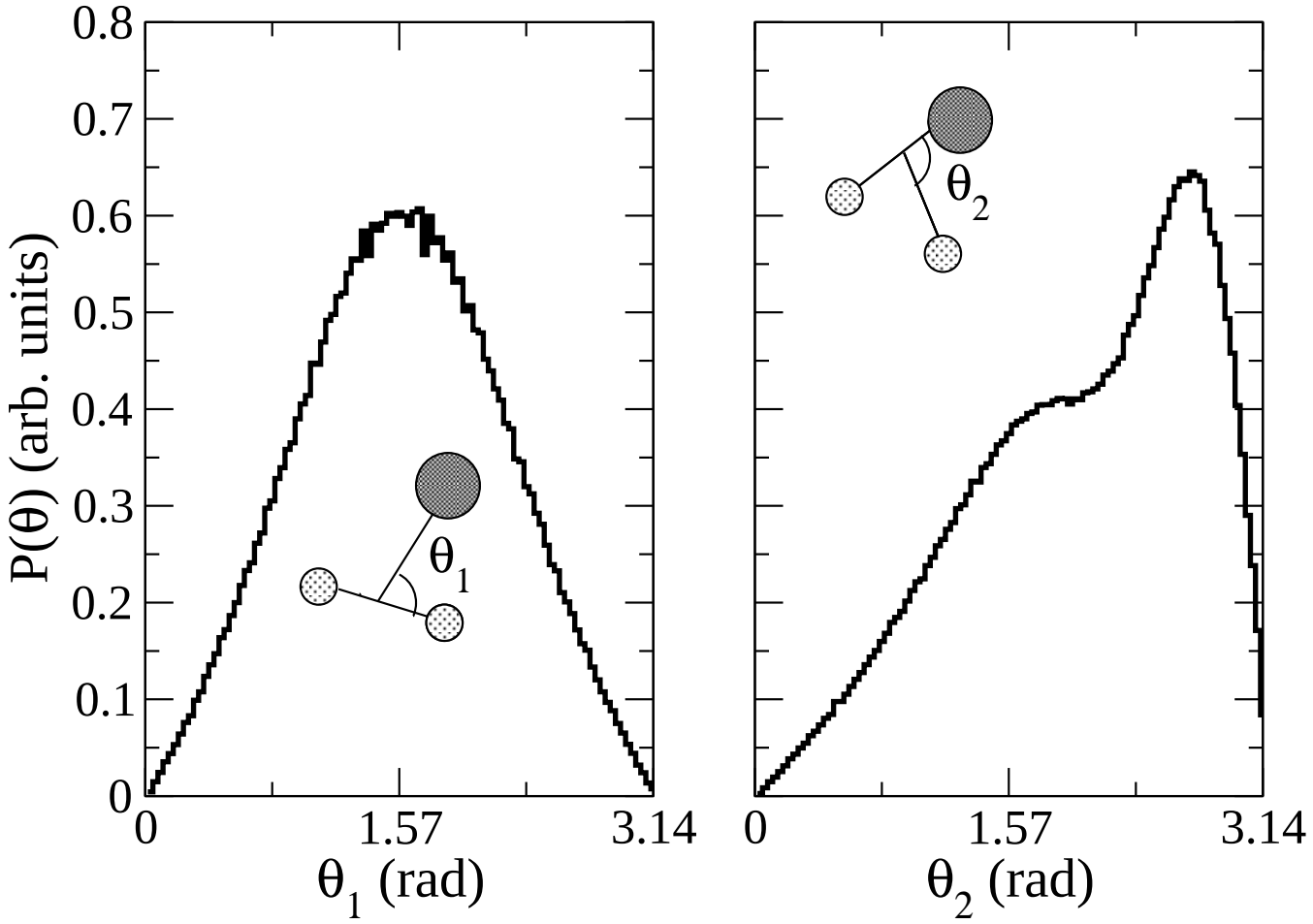

Figure 43: The angular distributions of the directions between two particles and their center of mass and the third particle for the 0^+ resonance of ^{6}Be. The two possible choices for the angle are plotted in each pannel.

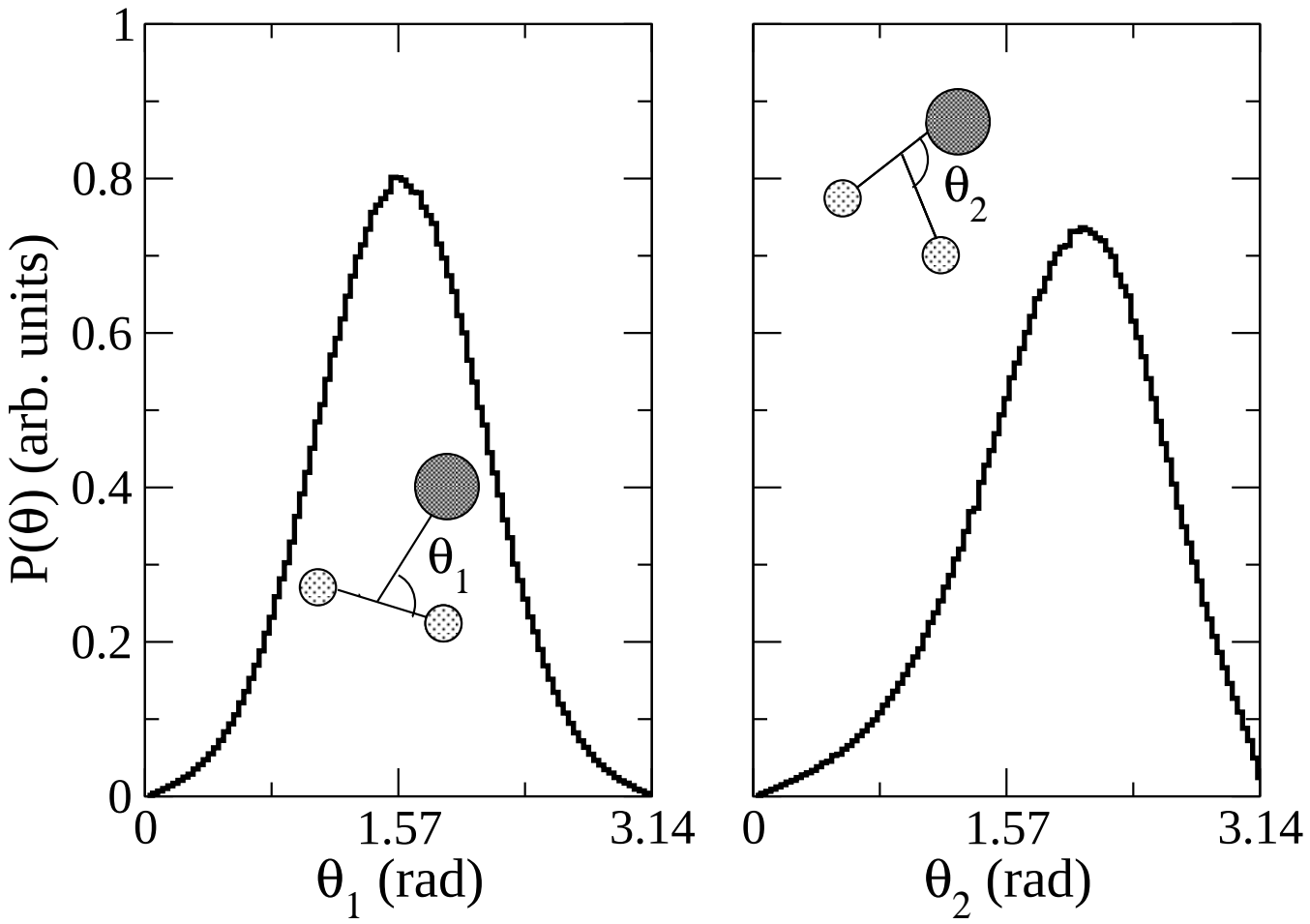

Figure 44: The angular distributions of the directions between two particles and their center of mass and the third particle for the 2^+ resonance of ^{6}Be. The two possible choices for the angle are plotted in each pannel.

References

[1] D. V. Fedorov and A. S. Jensen,
Efimov effect in coordinate space Faddeev equations,
Phys. Rev. Lett. **71**, 4103 (1993).

[2] A.S. Jensen, E. Garrido and D.V. Fedorov,
Three-Body Systems with Square-Well Potentials in L=0 States, Few-Body Systems, **22**, 193-236 (1997).

[3] E. Nielsen, D.V. Fedorov, A.S. Jensen and E. Garrido,
The three-body problem with short-range interactions,
Phys. Rep. **347** (2001) 373-459.

[4] A.S. Jensen, K. Riisager, D.V. Fedorov and E. Garrido,
Structure and reactions of quantum halos,
Rev. Mod. Phys. **76** (2004) 215-261.

[5] D.V. Fedorov, E. Garrido, and A.S. Jensen,
Complex scaling of the hyper-spheric coordinates and Faddeev equations,
Few-body systems, **33** (2003) 153-171.

[6] A.S. Jensen and D.V. Fedorov,
Efimov states in asymmetric systems
Europhysics Lett. **62** (2003) 336-342.

[7] E. Garrido, D.V. Fedorov and A.S. Jensen,
Efimov effect in nuclear three-body resonance decays,
Phys. Rev. Lett. **96** (2006) 112501(4).

[8] E. Garrido, D.V. Fedorov, A.S. Jensen and H.O.U. Fynbo,
Anatomy of three-body decay:
I. Schematic models, Nucl. Phys. **A748** (2005) 27-38;
II. Decay mechanism and resonance structure, Nucl. Phys. **A748** (2005) 39-58;
III. Energy distributions, Nucl. Phys. **A 766** (2006) 74-96.

[9] E. Garrido, D.V. Fedorov, H.O.U. Fynbo and A.S. Jensen
Energy distributions of charged particles from three-body decay
Nucl. Phys. **A 781** (2007) 387.

[10] E. Garrido, D.V. Fedorov, H.O.U. Fynbo and A.S. Jensen
Isospin mixing and energy distributions in three-body decay
Phys. Lett. **B 648** (2007) 274-278

[11] R. Alvarez-Rodriguez, E. Garrido, A.S. Jensen, D.V. Fedorov, and H.O.U. Fynbo
Structure of low-lying ^{12}C-resonances
Eur.Phys.J. **A 31** (2007) 303

[12] R. Alvarez-Rodriguez, E. Garrido, A.S. Jensen, D.V. Fedorov, and H.O.U. Fynbo
Energy distributions from three-body decaying many-body resonances
Phys.Rev.Lett. **99**, (2007) 072503(4).

[13] R. de Diego, E. Garrido, D.V. Fedorov, A.S. Jensen
Neutron-^{3}H potentials and the ^{5}H-properties
Nucl. Phys. **A786** (2007) 71-89.

[14] R. de Diego, E. Garrido, D.V. Fedorov, A.S. Jensen
Cluster sum rules for three-body systems with angular-momentum dependent interactions
Phys. Rev. **C 77** , 024001(10p) (2007).

[15] C. Romero-Redondo, E. Garrido, D.V. Fedorov and A.S. Jensen
Isomeric 0^- halo-state in ^{12}Be and ^{11}Li
Phys. Lett. **B 660** (2008) 32-36.

[16] C. Romero-Redondo, E. Garrido, D.V. Fedorov and A.S. Jensen
Three-body structure of low-lying ^{12}Be states
Phys. Rev. **C77** (2008) 054313 (1-15).

[17] Álvarez-Rodríguez, H.O.U. Fynbo, A.S. Jensen, E. Garrido,
On the distinction between sequential and direct three-body decays
Phys.Rev.Lett. **100** (2008) 192501(4).

[18] R. Álvarez-Rodríguez, A.S. Jensen, E. Garrido, D.V. Fedorov, H.O.U. Fynbo
Momentum distributions of α-particles from decaying low-lying ^{12}C-resonances
Phys.Rev. **C77**, (2008) 064305.

[19] E. Garrido, A.S. Jensen and D.V. Fedorov
Necessary conditions for accurate computations of three-body partial decay widths
Phys.Rev. **C 78** (2008) 034004 (1-12).

[20] P. Papka et al., Decay path measurements for the 2.429 MeV state in ^{9}Be Phys. Rev. **C 75** (2007) 045803.

[21] R.H. Dalitz, Philosophical mag. **44**, 1068 (1953).

[22] C. Amsler, Rev. Mod. Phys. **70**, 1293 (1998).

[23] U. Galster, U. Müller, H. Helm, Phys.Rev.Lett. **92**, 073002 (2004).

[24] U. Galster et al., Phys.Rev. **A72**, 062506 (2005).

[25] B. Blank et al., C. R. Physique **4**, 521 (2003).

[26] H.O.U. Fynbo et al., Phys.Rev.Lett. **91**, 082502 (2003).

[27] C. Aa. Diget et al., Nucl. Phys.**A 760**, 3 (2005).

[28] E. Garrido, D.V. Fedorov, H.O.U. Fynbo and A.S. Jensen, Nucl. Phys. **A 781**, 387 (2007).

[29] D.V. Fedorov, E. Garrido, and A.S. Jensen, Few-body systems, **33**, 153 (2003).

[30] E. Garrido, D.V. Fedorov, A.S. Jensen and H.O.U. Fynbo, Nucl.Phys.**A 766**, 74 (2005).

[31] M. Freer et al., Phys. Rev. **C49**, 1751R (1994)

[32] C. Aa. Diget, PhD-thesis, IFA, University of Aarhus, 2006.

[33] Y. Kanada-En'yo, Phys. Rev. Lett. **81**, 5291 (1998).

[34] T. Neff and H. Feldmeier, Nucl. Phys.**A 738**, 357 (2004).

[35] P. Descouvemont, Nucl. Phys.**A 709**, 275 (2002).

[36] S.C. Pieper, Nucl. Phys.**A 751**, 516 (2005).

[37] P. Navratil, J.P. Vary, and B.R. Barrett, Phys. Rev. **C 62**, 054311 (2000).

[38] D. V. Fedorov and A. S. Jensen, Phys. Lett. **B389**, 631 (1996).

[39] S. Ali and A.R. Bodmer, Nucl. Phys. **80**, 99 (1966).

[40] R. Álvarez-Rodríguez, E. Garrido, A.S. Jensen, D.V. Fedorov, and H.O.U. Fynbo, Eur.Phys.J.**A 31** (2007) 303.

[41] B.V. Danilin et al., *Sov. J. Nucl. Phys.* **46**, 225 (1987).

[42] F. Ajzenberg-Selove, Nucl. Phys. **A560** (1990) 1,
and http://www.tunl.duke.edu/nucldata/chain/12

[43] E. Garrido, D.V. Fedorov and A.S. Jensen, Nucl. Phys. A **708**, 277 (2002).

[44] E. Garrido, D.V. Fedorov, and A.S. Jensen, Nucl. Phys. A **733**, 85 (2004).

[45] L.V. Grigorenko, I.G. Mukha, and M.V. Zhukov, Nucl. Phys. A **713**, 372 (2003).